Universidad del País Vasco
Euskal Herriko Unibertsitatea
ZIENTZIA ETA TEKNOLOGIA FAKULTATEA
FACULTAD DE CIENCIA Y TECNOLOGÍA

Bachelor Final Project
Chemical Engineering

MnO_x-CeO_2 as an alternative catalyst for the simultaneous abatement of NO_x and PCDD/Fs from MSW treatment plants

Feasibility and reaction pathways study

Author:
Antton Ibarbia
Director:
Asier Aranzabal
Co-director:
Miren Gallastegi Villa

Leioa, 27th June 2017

Universidad del País Vasco
Euskal Herriko Unibertsitatea
ZIENTZIA ETA TEKNOLOGIA FAKULTATEA
FACULTAD DE CIENCIA Y TECNOLOGÍA

Bachelor Final Project
Chemical Engineering

MnO_x-CeO_2 as an alternative catalyst for the simultaneous abatement of NO_x and PCDD/Fs from MSW treatment plants

Feasibility and reaction pathways study

Author:
Antton Ibarbia
Director:
Asier Aranzabal
Co-director:
Miren Gallastegi Villa

Leioa, 27th June 2017

TABLE OF CONTENTS

1 INTRODUCTION

Due to the consumerism of the modern society, the excessive generation and environmentally safe disposal of solid waste has become one of our biggest challenges. In order to address this, different strategies are being promoted depending on the legislation of each country. In Spain, the Municipal Solid Waste (MSW) management strategy is defined in the 22/2011 Law (Ley 22/2011,), which states that prevention is the best option, followed by reutilization, recycling, other valorization methods and, finally, destruction. This strategy is widely accepted worldwide, but there are some discrepancies in the way to approach the last step, the destruction of the non-recyclable waste. The traditional and most used method is to dispose the waste in landfill sites, but lately incineration is taking hold. In fact, some countries, such as Germany, virtually incinerate all their non-recyclable waste (Waste-to-Energy Research and Technology Council, 2017).

Incineration seems to be a good alternative to landfill sites, since it reduces the volume of the waste up to a 90% and eliminates certain infectious components. Municipal Waste Incineration (MWI) plants are reported to be highly hygienic (Hou et al., 2014) and are immediately effective in terms of transport, since MWI plants can be located close to waste sources. Moreover, through the waste-to-energy processes, incineration can be used to produce electricity and heat for nearby buildings. This electricity is much cleaner than energy generated from burning fossil fuels. For instance, in the EU 11 million tons of CO_2 emissions are saved annually through the substitution of fossil fuels by energy production from waste-to-energy MWI plants (Reimann, 2013).

Nevertheless, the emissions of many hazardous substances make MWI plants unpopular. The gases at the exhaust flue gas of a MWI are mainly composed of water (H_2O), nitrogen (N_2), carbon dioxide (CO_2) and oxygen (O_2); but they also contain particulate material (ash and metals) and gaseous pollutants, such as nitrogen oxides (NO_x), acid gases (SO_2, HF, HCl), hydrocarbons, Volatile Organic Compounds (VOC), dioxins (PCDD) and furans (PCDF). These hazardous substances are environmentally harmful, causing acid rain, photochemical contamination of the troposphere and ozone layer destruction, among other environmental problems (Dvořák et al., 2010; Kang et al., 2007). Furthermore, many VOCs, PCDDs and PCDFs have been proved to be carcinogenic and some have direct systemic toxicity (International Agency for Research on Cancer, 2017).

Therefore, from the environmental perspective, the outlet gas purification line is the most important part of MWI plants. In this regard, modern technology is able to meet current legislative limit values of emissions and the cost of operation of incineration can be offset by energy sales in waste-to-energy thermal power plants (Brunner, 1994). The emission limit values of European MWI plants are set in the Waste Incineration Directive (Directive 2000/76/EC). These values are given in Table 1, together with typical average concentration values of pollutants at the outlet of the combustion chamber. The Directive 2000/76/EC also sets the operational conditions, technical requirements and controls on releases to water; aiming to lessen the risks which MWI plants pose to human health.

Table 1. Average concentration of combustion products at the outlet of the combustion chamber (based on 11% O_2) and emission limit values for MWI plants (Directive 2000/76/EC).

Component	**Unit**	**Combustion chamber outlet**	**Daily limit 2000/76/EC**
Particulate material	mg/m^3_N	1000-5000	10
Mercury	mg/m^3_N	0,05-0,5	0,05
Cadmium + Talium	mg/m^3_N	< 3	0,05
Other heavy metals (Pb, Sb, As, Cr, Co, Cu, Mn, Ni, V, Sn)	mg/m^3_N	< 50	0,5
Fluorinated organic compounds (as HF)	mg/m^3_N	5-20	1
Chlorinated organic compounds (as HCl)	mg/m^3_N	500-2000	10
Sulfurous compounds (as SO_2)	mg/m^3_N	200-1000	50
NO_x (as NO_2)	mg/m^3_N	250-500	200
Nitrous oxide (N_2O)	mg/ m^3_N	< 40	n/a
CO	mg/ m^3_N	5-50	50
CO_2	%v	5-10	---
H_2O	%v	10-20	---
O_2	%v	---	---
Total Organic Carbon (TOC)	mg/m^3_N	1-10	10
PCDD/Fs	$mg\ TEQ/ m^3_N$	0,5-10	0,1

In order to comply with the legislative limits and discharge the minimum quantity of hazardous compounds, the combustion gases of MWI plants are treated through different separation processes. These usually include:

- Electrostatic precipitator for the elimination of solid particles
- Fabric filters for the elimination of solid PCDD/Fs and vapor associated with particles.
- Dry and wet scrubbers to remove acid gas and particles.
- Dry sorbent injection to reduce acid gas emissions.
- Entrained flow adsorber which recirculates an adsorbent until it is exhausted and burned.
- Circulating fluidized bed of fine-grained heat-oven coke and an additive that can simultaneously absorb HCl, HF and SO_2.
- Moving-bed adsorber which is used as an alternative to fixed bed adsorbers that can be blocked due to moisture.
- Selective catalytic reactor for elimination of NO_x.

It is noteworthy that the latter process (catalytic reactor for elimination of NO_x) has been introduced in recent years and even though its use is desirable, still few MWI plants have implemented it.

Among all pollutants emitted from MWI plants, NO_x and PCDD/Fs are the ones for which catalytic destruction technology is the most appropriate. Up to now, the most used technology for the abatement of NO_x from the combustion gases of MWI plants has been the non-catalytic reaction with ammonia. However, this technique is outdated, since environmental laws are

becoming increasingly strict, especially regarding emissions, requiring lower concentrations and harmfulness in exhaust gases (Directive 2000/76/EC). Therefore, MWI plants are keen on more effective methods for the removal of pollutants from MWI plants' combustion gases, not only aiming to obey environmental laws, but also to improve the public image of incinerators. In this sense, the Selective Catalytic Reduction (SCR) using vanadium-based catalysts is a suitable alternative. Although many competitive reactions occur in parallel with the SCR reaction creating unwanted products (Busca et al., 1998; Brandenberger et al., 2008), authors agree that its stoichiometry is the following.

$$4\ NH_3 + 4\ NO + O_2 \rightarrow 4\ N_2 + 6\ H_2O \quad (1)$$

On the other hand, PCDD/Fs are usually set aside by physical containment methods, for instance, using activated carbon filters. However, these adsorption- and absorption-based techniques transfer PCDD/Fs from the gas phase to solid or liquid phases which require further inertization treatments (Liu et al., 2012). This is why catalytic technologies are preferable for their removal at the source of emission through Catalytic Total Oxidation (CTO), destructing hazardous molecules to form carbon oxides and HCl as shown hereafter (Debecker et al., 2007; Finocchio et al., 2006; Goemans et al., 2003; McKay, 2002).

$$C_{12}H_nCl_{8-n}O_2 + (9+0.5\ n)\ O_2 \rightarrow (n-4)\ H_2O + 12\ CO_2 + (8-n)\ HCl \quad (2)$$

$$C_{12}H_nCl_{8-n}O + (9.5+0.5\ n)\ O_2 \rightarrow (n-4)\ H_2O + 12\ CO_2 + (8-n)\ HCl \quad (3)$$

1.1 SIMULTANEOUS ABATEMENT OF NO_x AND PCDD/Fs

In the past years, numerous studies have been carried out on the low-temperature abatement of NO through SCR using a wide variety of catalysts. Research has specially focused on transition metal oxide VO_x/TiO_2 catalyst, which is currently the commercial catalyst for SCR with NH_3. It has been found out that this catalyst is also suitable for the abatement of PCDD/Fs (Debecker et al., 2007; Albonetti et al., 2008; Wang et al., 2015; Wielgosiński et al., 2007). In fact, when comparing four MWI plants in Taiwan, Wang et al. (2007) found out that PCDD/Fs emissions were significantly lower at the plants equipped with SCR catalytic reactors. Therefore, the research group Chemical Technologies for Environmental Sustainability (TQSA), in which the present Bachelor Final Project has been carried out, proposes the simultaneous abatement of NO_x and PCDD/Fs using catalytic technology (dDiNOx process).

In recent years, research has evidenced the feasibility of the dDiNOx process over the commercial VO_x/TiO_2 catalyst, since acceptable conversions of both pollutants have been obtained in the temperature range of 200-350 ºC (Gallastegi-Villa, 2016; Goemans et al., 2003; Jones and Ross, 1997; Xue et al., 2013). This research is in its initial stages and there is very limited literature about it, mainly due to the complicated nature of the process. Most authors have studied the reactions independently, but it has been proved that SCR and CTO reaction are interconnected in the dDiNOx process (Gallastegi-Villa, 2016). The efficiency of NO_x and PCDD/Fs removal is different when reactions are carried out separately and simultaneously. In spite of this breakthrough, reaction pathways and the relationships between them cannot still be fully described.

In order to carry out the dDiNOx process in MWI plants, different dispositions are possible to set a catalytic reactor. In order to avoid further de-novo formation (McKay, 2002) of PCDD/Fs, the so called Tail-End (Figure 1) disposition is the most appropriate. However, the flue gas temperature is around 180 ºC and therefore, with the commercial catalyst, the gas needs to be

re-heated in order to achieve the optimum catalytic temperature (Forzatti et al., 2012; Gallastegi-Villa, 2016), significantly incrementing operational costs. Nonetheless, using Tail-End configuration dust particles are eliminated before the reactor preventing catalyst deactivation, broadening the choice of possible catalysts.

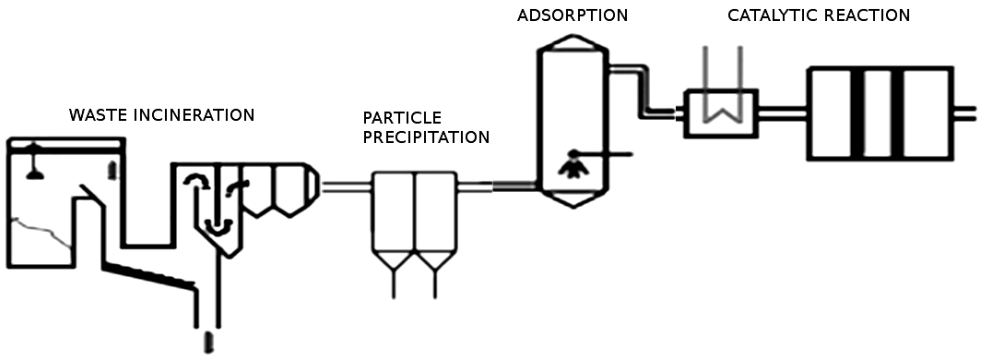

Figure 1. Tail-End disposition of the dDiNOx unit.

1.2 STATE OF THE ART OF THE dDiNOx PROCESS

As mentioned previously, the commercial catalyst used in MWI plants for NO_x abatement is VO_x/TiO_2. VO_x is used as the active site, due to its variety of possible oxidation states (from +2 to +5) and structural variety (Wachs et al., 2003; Khodakov et al., 1999). The support has a big influence on the formed VO_x structures, being TiO_2 ideal to form highly dispersed and very active VO_x structures (Boningari et al., 2013; Busca et al., 1998). This leads to an excellent catalytic activity for SCR with NH_3.

It is known that vanadium oxides can form many structures with different catalytic activity and behavior (Wachs, 1990; Wachs, 2011), represented in Figure 2.

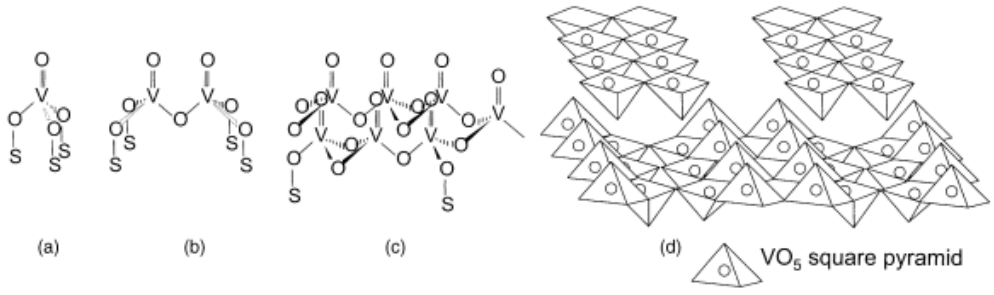

Figure 2. Molecular configurations of supported vanadium oxides (being S the support cation): (a) isolated vanadium oxide species; (b) dimeric vanadium oxide species; (c) two-dimensional vanadium oxide chains; (d) V_2O_5 crystals.

Catalytic studies for many different oxidation reactions have demonstrated that the monomeric and polymeric surface species are generally the most active sites in supported VO_x catalysts, since the crystalline phases have fewer exposed active surfaces (Giakoumelou et al., 2006; Wachs et al., 1996).

Regarding the dDiNOx process, Gallastegi-Villa (2016) proved that, generally, monomeric (isolated) VO_4 species are the most active for o-DCB oxidation (model molecule of PCDD/Fs), due to the strength and abundance of Lewis type acid sites. Contrarily, polymeric and square

pyramidal species were found to be the most active in the SCR reaction. This can be attributed to the proximity of acid and redox sites participating in the reaction mechanism and to their Brønsted type acidity.

When it comes to reaction pathways, at low temperature, the presence of NO and NH_3 improves the CTO performance, being o-DCB conversion higher in the presence of SCR gasses than in absence. It has been proven that the beneficial effect is associated to NO, since NO_2 formed from NO oxidation has higher oxidation potential than O_2, and it may re-oxidize vanadium and promote the oxidation of intermediate aromatic compounds (Bertinchamps et al., 2005; Dvořák et al., 2010).

Unfortunately, high o-DCB conversion is only achieved at high temperatures, when the reaction mechanism changes and this pollutant is also adsorbed in polymeric and crystalline species. Therefore, at high temperature, o-DCB and NH_3 compete for the same active sites (Brønsted acid sited), leading to a decrease of NO conversion, and having a detrimental effect on the dDiNOx process (Gallastegi-Villa, 2016). NO conversion further decreases because of parallel reactions taking place at higher temperatures, such as NH_3 oxidation.

In general, acceptable conversion of both pollutants occurs in a narrow temperature range, from 285 to 330 ºC (Gallastegi-Villa, 2016). Moreover, the oxidation of o-DCB in polymeric species gives rise to unwanted partial oxidation byproducts, such as dichloromaleic anhydride (DCMA). These are major drawbacks that may keep the dDiNOx process over VO_x/TiO_2 catalyst from being implemented in the industry, and therefore, alternative catalysts should be considered, among which MnO_x-CeO_2 catalyst stands out due to its excellent properties.

1.3 MnO_x-CeO_2 CATALYST FOR THE dDiNOx PROCESS

Recently, MnO_x based catalysts are gaining much attention as low temperature oxidation catalysts. They are a promising alternative to the commercial catalyst for both NO_x SCR with NH_3 and PCDD/Fs oxidation. The excellent oxidizing behavior is mainly attributed to its variable valences and various types of labile oxygen. There are many factors that influence the catalytic activity of MnO_x.

Mn is a multivalent element that forms several stable oxides. The activity of the Mn oxides is correlated to amount of surface oxygen, being MnO_2 the most active and MnO the least (Kapteijn et al., 1994). However, Mn_2O_3 is preferred for SCR reaction due to its high selectivity towards N_2 formation. Compared to MnO_2, Mn_2O_3 has higher Mn-O bond energy, and therefore, less N-H bonds of NH_3 are broken to form less N-species such as N_2O (Tang et al., 2010).

Crystallinity of the MnO_x based catalyst also plays a major role in the performance of the catalyst. Amorphous MnO_x generally exhibits higher catalytic activity at low temperatures compared to highly crystallized MnO_x (Tang et al., 2007). Crystallinity mainly depends on the preparation method, being sol-gel and precipitation methods the most effective to form highly amorphous structures (Tang et al., 2006; Wu et al., 2007b).

Therefore, better catalytic performance should be expected from an amorphous catalyst with high surface area and high oxygen content species on its surface. At this point, it should be pointed out that the factors influencing the catalytic activity are sometimes interconnected and it is difficult to establish the relative importance of this factors.

Despite bulk MnO_x catalysts show impressive activity at low temperatures, there are also big drawbacks. These catalysts tend to deactivate when in contact with SO_2 and/or H_2O, and significant amounts of N_2O are usually formed at higher temperatures (Liu et al., 2016). One way to tackle these problems is to synthesize multi-metal oxide mixed catalysts, which may also exhibit higher catalytic activity.

Among these, MnO_x-CeO_2 is the most prominent due to its abundant oxygen reservoir. When CeO_2 is used as catalyst, the redox shift between Ce^{4+} and Ce^{3+} leads to the formation of oxygen vacancies on the surface. In these vacancies gaseous oxygen may be chemisorbed, specially enhancing the oxidation of NO to NO_2 at low temperatures (Liu et al., 2013; Wei et al., 2015), which is beneficial for the SCR process, as will be explained later on. Moreover, an amorphous solid solution may arise from the incorporation of Mn ions into the CeO_2 lattice (Tang et al., 2006; Jampaiah et al., 2015). Gallastegi-Villa (2016) evaluated different manganese-based catalysts for the dDiNOx process and concluded that MnO_x-CeO_2 had the best performance.

Regarding reaction mechanisms, it has been proven that both NO and NH_3 are adsorbed on the surface of MnO_x-CeO_2 catalysts (Eigenmann et al., 2006). Various hypotheses have been proposed for the mechanism of the SCR reaction. Some researchers believe that NH_3 is first adsorbed in Lewis acid centers forming intermediates like NH_2 and adsorbed NH_3, which then react with gas phase O_2, NO and NO_2, according to Eley-Rideal (ER) mechanism (Marbán et al., 2004; Eigenmann et al., 2006). Others claim that the reaction takes places preferentially through Langmuir-Hinshelwood (LH) mechanism, where adsorbed NH_3 reacts with an activated nitrite intermediate adsorbed on the surface (Xu et al., 2013; Qi et al., 2004; Wu et al., 2007a).

In the case of the oxidation of chlorinated aromatic compounds, very little research works report data on reaction mechanism. But it is extensively accepted that the catalytic combustion of organic compounds over transition metal oxides, involves a Mars-Van Krevelen (MVK) mechanism, where the adsorbed organic molecules are primarily oxidized by the lattice oxygen of metal oxides. Accordingly, when analyzing the oxidation of chlorobenzene over MnO_x-CeO_2 catalyst, Sun et al. (2016) proposed that chlorobenzene oxidation route is initiated from its adsorption in acid sites, which is then oxidized by active lattice oxygen species into CO_2 and H_2O. In the same work, a wide range of aldehyde-type (chlorinated and unchlorinated) byproducts were detected when the same catalyst was impregnated over H-ZSM5 zeolite (Sun et al., 2016). This evidences that the reaction mechanism is strongly dependent on the structure and morphology of the catalyst.

Considering all the above mentioned, MnO_x-CeO_2 mixed oxide catalysts were selected as an alternative to the commercial VO_x/TiO_2 for the dDiNOx process. Gallastegi-Villa (2016) proved the feasibility of the process over this catalyst and achieved significantly higher conversions than the commercial catalyst, especially at low temperatures. This is a big advantage for industrial applications, since the reduction of the process temperature results in substantial cost reductions. Also, Gallastegi-Villa (2016) determined that the optimum Mn/Ce molar ratio is about 85/15. Therefore, for the sake of the present work, MnO_x-CeO_2 catalyst with a molar ratio of 85/15 was chosen to study the dDiNOx process; comparing to the commercial catalyst and analyzing whether interaction between SCR and CTO reactions, like for VO_x/TiO_2, exist.

Co-precipitation method was selected for the preparation of the catalyst. The catalysts prepared with this method are usually very active, since it promotes the formation of mixed oxides with strong synergetic interactions between Mn and Ce metals (Cui et al., 2013).

1.4 EFFECT OF WATER ON THE dDiNOx PROCESS

Up to date, there are no publications analyzing the influence of water on the dDiNOx process, mainly because of the scarce amount of works on this subject and the complexity of the process. However, this is a very important point, since 10-20% H_2O in volume should be expected at the outlet of a MSW combustion chamber. Therefore, the catalyst would be continuously in contact with H_2O in a real life application and should be resistant to it.

Water vapor may partially deactivate the catalyst due to the decrease of available active sites. It should be pointed out that even in completely dry flue gas conditions, water generated in SCR reactions may deactivate the catalyst (Liu et al., 2016). This deactivation may be reversible or irreversible. The reversible deactivation is generally attributed to the competitive adsorption of H_2O and reactants, such as NH_3 and NO. Adsorbed water occupies some active sites, decreasing the number of available active sites for the reactants, consequently decreasing NO conversion. However, the inhibition effect disappears at higher temperatures, at which water is desorbed. On the other hand, the adsorbed water may dissociate on the catalyst surface, causing irreversible deactivation due to the formation of surface hydroxyls (-OH). These groups can only be eliminated at very high temperatures, and after cutting H_2O off the activity is not recovered at lower temperatures (Liu et al., 2016).

The effect of water has been studied in independent SCR and CTO reactions over manganese-based catalysts. Most researchers agree that water has a mild detrimental and mostly reversible effect on the SCR reaction over MnO_x-CeO_2 catalysts (Qi and Yang, 2003; Chen et al., 2015). Also, water may enhance the selectivity towards N_2, since it inhibits the non-selective NH_3 oxidation at high temperatures (Qi et al., 2015). In contrast, the commercial VO_x/TiO_2 catalyst has been reported to suffer severe and reversible deactivation under humid conditions (Huang et al., 2002; Nova et al., 2000).

Regarding the oxidation of PCDD/Fs, it has been repeatedly observed that the presence of water decreases the activity of manganese- and cerium-based catalysts. Sun et al. (2016) reported that MnO_x-CeO_2 catalyst undergoes severe deactivation when temperature exceeds 250 ºC. This was attributed to the competitive adsorption between H_2O and chlorobenzene, also reported in other publications (Dai et al., 2013; Dai et al., 2012; He et al., 2015). Another hypothesis is that water could remove some of the Brønsted acid sites involved in the oxidation of chlorobenzene, resulting in a lower activity (Bertinchamps et al., 2006; Sun et al., 2016). In addition, water has been reported to promote the ring opening reaction of chlorobenzene, either increasing the conversion at low temperature (Hetrick et al., 2011) or yielding more primary chain by-products (Sun et al., 2016). This is attributed to the removal of Cl species accumulated on the catalyst surface by water, producing HCl according to the reverse Deacon reaction:

$$H_2O + Cl^- \leftrightarrows HCl + OH^- \quad (4)$$

2 OBJECTIVES

Two main goals can be described for the purpose of this project. The first one is to evaluate the feasibility of the simultaneous abatement of NO_x and PCDD/Fs over MnO_x-CeO_2 catalyst, which is a promising alternative to the commercial VO_x/TiO_2. The other main goal is to evaluate the reaction pathways of the process in order to propose a suitable reaction scheme.

For the compliance of these objectives, the following milestones are proposed:

- Preparation of MnO_x-CeO_2 catalyst with 85:15 Mn/Ce molar ratio and its characterization in order to be able to predict and explain the behavior of the catalyst.

- Evaluation of the feasibility of the simultaneous abatement, considering the activity, selectivity and durability of MnO_x-CeO_2 catalyst and comparison to the commercial VO_x/TiO_2.

- Identification of the side reactions taking place in the process from which unwanted products may arise.

- Evaluation of interactions between o-DCB oxidation and NO reduction and identification of the effect of the concentration of different compounds (o-DCB, NO, NH_3 and H_2O) on the dDiNOx process.

- Determination of the effects of reactant concentrations in the conversion and selectivity, including the influence of water in the process.

- Proposal of a reaction scheme that the dDiNOx process may follow over MnO_x-CeO_2.

3 MATERIALS AND METHODS

3.1 CATALYSTS' PREPARATION

In this work, MnO_x-CeO_2 catalyst was prepared by a standard co-precipitation method. An aqueous solution of the precursor salts was prepared by dissolving calculated amounts cerium (III) nitrate $Ce(NO_3)_3{\cdot}6H_2O$ (99%, Sigma-Aldrich) and manganese (II) nitrate $Mn(NO_3)_2{\cdot}4H_2O$ (98.5%, Merck) to obtain a molar ratio of 85/15 in the final catalyst. An excess solution of ammonium carbonate $(NH_4)_2CO_3$ (99.5%, Merck) was added slowly to the solution with vigorous stirring until pH corresponding to complete precipitation (in the range of 8.8-9). The mixture was stirred for 2 h and aged for 20 h at room temperature and constant pH, as this may result in a more active catalyst (Picasso et al., 2015). Then, the precipitate was filtered and washed several times with distilled water until pH was constant. The obtained solid was dried at 110 ºC in air overnight and calcined at 500 ºC in a convective oven for 3 h. Finally, the catalyst was crushed and sieved to 0.3 - 0.5 mm. The catalyst is denoted as MnO_x-CeO_2. Pure MnO_x and CeO_2 catalysts were also prepared by the precipitation method, following the same procedure, but using the correspondent precursor salt.

3.2 CATALYSTS' CHARACTERIZATION

The physical and chemical properties of the synthesized catalysts were determined using various characterization techniques.

3.2.1 Chemical composition

The actual amount of Mn and Ce in the prepared MnO_x-CeO_2 catalyst was characterized by Inductively Coupled Plasma Atomic Emission Spectroscopy, ICP-AES (Horiba Jobin Yvon, Activa). In order to prepare appropriate samples for the test, samples of the powered catalysts were completely dissolved in a solution of 1:3 molar solution of HNO_3:HCl, nitric acid to hydrochloric acid, in a microwave apparatus (CEM Mars Xtraction).

3.2.2 Textural properties

The textural properties of MnO_x-CeO_2 were evaluated by N_2 adsorption–desorption isotherms at -196 °C, in a Micromeritics TRISTAR II 3020 apparatus. Specific surface areas of the prepared samples were determined by the standard Brunauer-Emmett-Teller (BET) procedure, using adsorption branch data in the relative equilibrium pressure (P/P_0) range of 0.03–0.3. Average pore size and distribution were calculated using the Brunauer-Joyner-Halenda (BJH) method from the desorption branch. The samples (15–20 mg) were previously degassed under nitrogen flow at 350 °C and atmospheric pressure for 4 h.

3.2.3 Crystal structure

The crystal structure of the prepared catalysts was evaluated using X-ray diffraction (XRD), conducted on a Philips PW 1710 X-ray diffractometer with CU Kα radiation (λ = 1.5406 Å) and Ni filter. The finely grounded samples were scanned between 10° and 80° (2θ) with 0.02°/s sampling interval. Phases were identified by comparison with JCPDS (Joint Committee on Powder Diffraction Standards) database cards.

Based on XRD diffractograms, it is possible to calculate the size of crystals in the internal structure of the catalyst using the Scherrer equation:

$$\tau = \frac{K\,\lambda}{\beta\cos\theta} \qquad (5)$$

Equation (5) is limited to particles larger than 3-4 nm, since the ones below this size are virtually transparent to X rays (Gallezot, 1984). λ refers to the X ray wavelength and θ to the incidence angle. K is the form factor and β the corrected Full Width at Half Maximum (FWHM) ($\beta=B^2-b^2$), being B the experimental width and b a correction due to the use of a machine.

3.2.4 Redox behavior

The redox properties of the catalysts were analyzed by Temperature Programed reduction using H_2 (H_2-TPR). The experiments were conducted on a Micromeritics AutoChem 2920 instrument. First, the samples (15–20 mg) were pre-treated under 50 cm^3/min of a 5% O_2/He mixture at 500 °C for 45 min, cooled down to room temperature and then flushed with helium for 60 min. Then, samples were heated from room temperature to 950 °C at a rate of 10 °C/min under 50 cm^3/min of 5% H_2/Ar. The water produced by reduction was trapped in a cold trap, and the consumption of H_2 was continuously monitored with a Thermal Conductivity Detector (TCD). The total H_2 consumption was calculated from time-integrated H_2-TPR curves.

3.2.5 Acidic properties

The acidic properties of the catalysts were characterized by NH_3 Temperature Programmed Desorption (NH_3-TPD). The experiments were conducted on a Micromeritics AutoChem 2910 instrument equipped with a TCD, gas mass flow controllers and an oven were a U shaped reactor is situated. First, the samples (15–20 mg) were pre-treated under 50 cm^3/min of a 5% O_2/He mixture at 500 °C for 45 min, and then cooled down to 40 ºC. Subsequently, NH_3 adsorption was carried out, with step feeds of 10% NH_3/He mixtures (5-6 cm^3/min) until sample saturation. Then, physically adsorbed NH_3 molecules were desorbed with a 50 cm^3/min He stream at 100 ºC for 2 h. The chemically adsorbed molecules were desorbed with the same He stream with increasing temperature until 550 ºC (10 ºC/min). The total acidity was calculated from time-integrated NH_3-TPD curves.

3.3 REACTION SET-UP

The reactions to evaluate the catalytic activity of the prepared MnO_x-CeO_2 catalysts in the $dDiNO_X$ process were carried out in a laboratory-scale reactor designed by the TQSA group. The flow diagram is represented in Figure 3, and can be divided into three parts: feeding system, catalytic reactor and analysis.

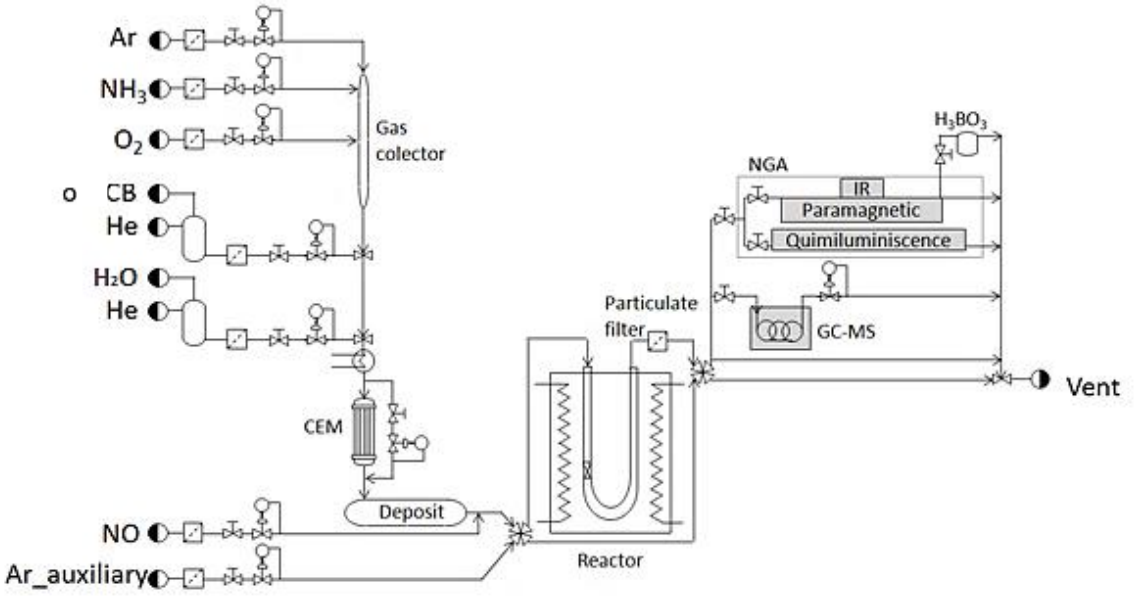

Figure 3. Flow diagram of the experimental reaction set-up.

3.3.1 Feeding

The reaction feeding was set to simulate MWI flue gas with tail-end configuration, according to the study carried out by Gallastegi-Villa (2016). Nominal concentration values in the feeding are shown in Table 2. Although combustion gases contain about 10% of CO_2, Gallastegi-Villa (2016) proved that the initial concentration of CO_2 has not a significant effect on the dDiNO$_X$ process over VO_x/TiO_2 catalysts. Therefore, for the purpose of being able to analyze the actual generation of CO_2, this compound was not feed to the reactor.

Regarding PCDD/Fs, there is a wide diversity of PCDD/Fs that can be found in the MWI exhaust gases. Unfortunately, working with these compounds in the laboratory is unviable due to their high toxicity and diversity of compounds with low concentrations. Therefore, model compounds are used in scientific studies which have to be structurally similar to PCDD/Fs, less toxic and easier to handle. The most used model compound, and the one used in the present project, is 1,2-dichlorobenzene or ortho-dichlorobenzene (o-DCB) (Saleh and Rahman, 2009; Ma et al., 2011); since it is composed of one aromatic ring and two chlorine atoms in the same positions as the most toxic PCDD/Fs, 2,3,7,8-tetrachlorodibenzodioxin (Albonetti et al., 2008).

Table 2. Nominal concentration values in the feeding.

Compound		Concentration
Nitrogen monoxide	NO	300 ppm
Ammonia	NH_3	300 ppm
Oxygen	O_2	10% (vol.)
Ortho-dichlorobenzene	o-DCB	100 ppm
Argon	Ar	Balance

In order to generate the feeding stream, the system is composed of four lines with gaseous compounds (Ar, O_2, NO and NH_3) and two lines for liquids o-DCB and H_2O. The piping is made of AISI-316 stainless steel to avoid o-DCB adsorption, and each line has a particle filter,

a two-port solenoid valve, a mass flow controller (Bronkhorst® High-Tech F-201CV) and a non-return valve. Liquid lines have different mass flow controllers (o-DCB: Bronkhorst® High-Tech µ-Flow L01-AGD-19-0-20S and H2O: Bronkhorst® High-Tech µ-Flow L13-AGD-11-K-10S) and instead of the non-return valve there are liquid-gas mixing valves. The gases, except NO, are initially mixed in a collector and o-DCB and water are delivered into the gas stream downstream.

The complete evaporation of the liquids and homogeneous blend of components was accomplished in a Bronkhorst® High-Tech W-102A-111-K controlled-evaporator-mixer (CEM). Furthermore, all pipelines were heated with electrical resistances to avoid gas adsorption or condensation. The resulting gas stream goes through a 25 L tank, made of AISI-314 stainless steel, in order to buffer potential oscillations of the o-DCB feeding concentration. The NO line is added after the tank, since there is evidence showing that NO could react with the material that the tank is made of.

In parallel to the feeding line, there is an auxiliary argon line to clean the pipeline and dry the catalyst bed. The four-port pneumatic valve allows the feeding stream or the argon to go through the reactor or bypass.

3.3.2 Reactor

The reactor consists of a fixed catalytic bed in a U-shaped tubular quartz reactor located inside convective-flow oven. The reactor has a 13.6 mm inside diameter, in order to ensure appropriate fluid-dynamic conditions and absence of diffusional control, checked beforehand by the TQSA group (Gallastegi-Villa, 2016). The catalytic fixed bed was mounted over calcined quartz wool, situated 15 mm above the inferior part of the reactor. The conditions to carry out the reactions are given in Table 3, which were set to guarantee a strictly kinematic regime (Gallastegi-Villa, 2016).

Table 3. Reaction conditions.

Variable	Value
Q (L_N/min)	2
d_p (mm)	0.3-0.5
W (g)	1.5
GHSV (h^{-1})	80000

The outlet of the reactor goes through a particle filter in order to avoid obstruction of the piping or analyzers. This line and the bypass are connected in a second four-port pneumatic valve, allowing the reaction products or the argon to go to the analyzers or venting.

3.3.3 Analysis

The reactor outlet stream is divided and fed to three inlets for composition analysis.

The first sub-stream is fed to an Agilent Technologies 7890A on-line gas chromatograph equipped with HP-VOC capillary column. A mass selective detector (MSD) 5975C is used to measure o-DCB concentration in the reactor inlet and outlet streams. Any other organic chlorinated compound that could form in the reaction is also measured. The established chromatograph method allows measurements every 7.5 minutes.

The second sub-stream is fed to NGA 2000 Rosemount Analytical analyzers where O_2 is measured by a paramagnetic detector and CO_2, CO and N_2O are analyzed by a Non Dispersive Infrared Detector (NDIR).

The third sub-stream is fed to a NGA 2000 CLD chemiluminiscence detector (CLD) which measures NO concentrations. All analyzer outlets are afterwards re-joined and sent to vent.

3.4 RECTION PROCEDURE

The reaction sequence consisted of various stages: calibration of the analysis equipment, stabilization of the feeding stream, concentration measurement, drying of the catalyst, and reaction.

In order to ensure correct concentration measurements, the analyzers were calibrated in every reaction sequence. The zero offsets and span factors of all gases were adjusted using reference streams with known concentrations.

The catalyst was initially dried with 1.5 L_N/min of argon (auxiliary stream) for approximately 2 hours to make sure surface water did not play a role in the reaction.

In parallel, the feeding stream was stabilized using the bypass. The o-DCB mass flow controller was activated once the piping was heated up to and the CEM module was at 190 °C, to avoid condensation. When all the feeding streams were stabilized at the set values, the second four-port valve switched positions, sending the feeding from bypass to analysis.

After the 2 hours of drying, the convective oven was cooled or heated up to the desired temperature. When all concentration measurements were stable, the first four-port valve switched positions, starting the reaction.

In order to study the dDiNOx reaction scheme thoroughly, feed composition was varied from one experiment to another, ranging the temperature in each reaction from 65 °C to 450 °C in a stepwise manner. Once a desired temperature was reached, it was kept constant until steady state conditions were achieved (stable conversions and product formations). Subsequently, the reactor was heated up to the next desired temperature. In addition, the effect of the feeding gas composition was analyzed, by changing the concentration of inlet gases during reactions, either from the beginning to the end of the experiment or injecting pulses of one reactant during experiments. A durability test of 40 h was also carried out and the effect of water on the process was also analyzed.

The catalytic activity was studied in terms of NO and o-DCB conversions:

$$x_A = \frac{c_{A0} - c_A}{c_{A0}} \cdot 100 \qquad (6)$$

4 RESULTS AND DISCUSSION

4.1 CATALYST CHARACTERIZATION

4.1.1 Chemical composition and textural properties

The chemical composition and textural properties of the prepared MnO_x-CeO_2 catalyst are summarized in Table 4. The final metal loading has been confirmed by means of ICP-AES analysis.

Table 4. Chemical composition and textural properties of MnO_x-CeO_2.

Nominal molar composition		Molar composition		Weight composition		S_{BET}	V_p
%Mn	%Ce	%Mn	%Ce	%Mn	%Ce	(m^2/g)	(cm^3/g)
85	15	85.45	14.55	48.28	51.72	107.7	0.31

The N_2 adsorption isotherm of the prepared catalyst is represented in Figure 4A. This is a type IV isotherm according to IUPAC, characteristic of mesoporous solids. The most characteristic feature of this isotherm is its hysteresis loop, which is associated with capillary condensation taking place in mesopores, and the limiting uptake over a range of high P/P_0. The hysteresis loop is classified as H1, where agglomerates or spherical particles are arranged in a fairly uniform way, with cylindrical pore geometry. This indicates a relatively high pore size uniformity and facile pore connectivity (Sing et al., 1985). The homogeneous pore size distribution is confirmed in Figure 4B, where a relatively narrow pore size distribution profile is observed, centered at ca. 6 nm.

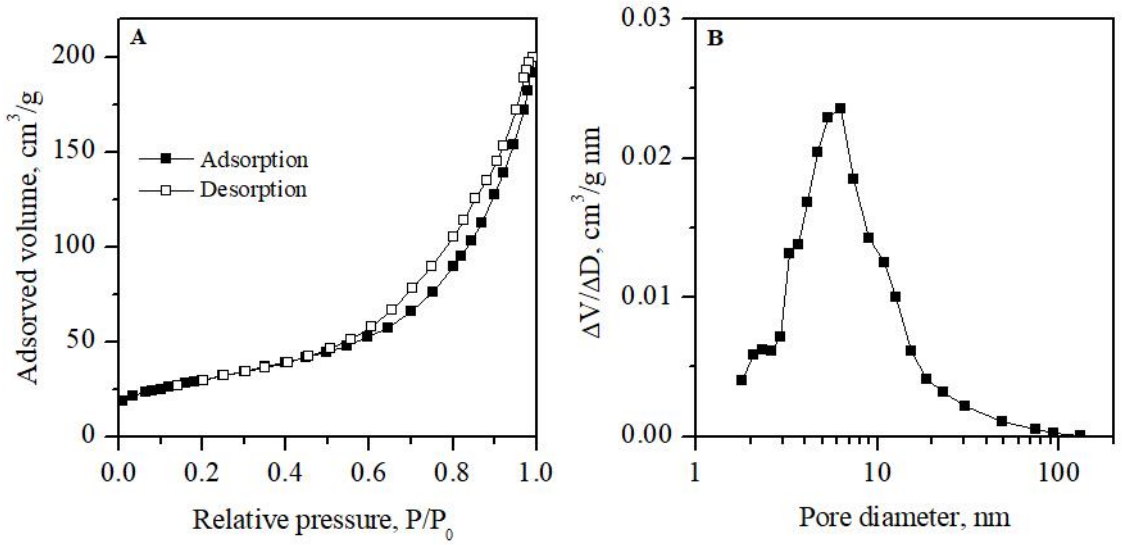

Figure 4. A) N_2 adsorption-desorption isotherms and B) pore size distribution of MnO_x-CeO_2.

4.1.2 Crystal structure

Figure 5 represents the results of XRD analysis of MnO_x-CeO_2 compared to reference MnO_x and CeO_2. CeO_2 diffractogram shows peaks at 2θ angles of 28.7°, 33.1°, 47.6°, 56.4° and 59.1°, which can be attributed to cerianite in form of cubic fluorite structure (JCPDS, 00-001-0800).

Sharp peaks corresponding to Mn_2O_3 and MnO_2 crystals can be observed in the reference MnO_x diffractogram.

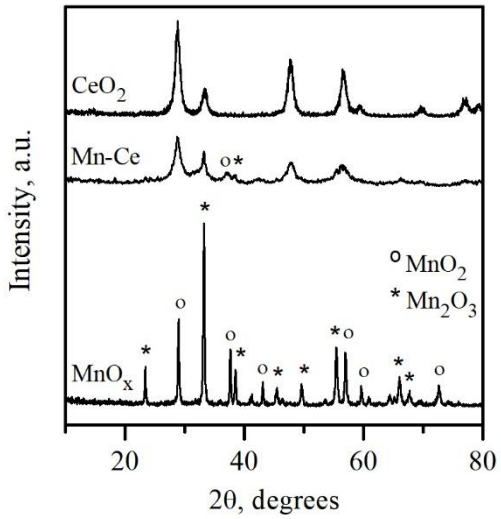

Figure 5. XRD diffractogram of MnO_x-CeO_2 compared to reference MnO_x and CeO_2.

The diffraction peaks in the MnO_x-CeO_2 sample are associated to fluorite, but their intensity is greatly reduced compared to pure CeO_2, indicating a smaller degree of crystallinity than pure MnO_x and CeO_2. This may indicate a high dispersion of MnO_x (Cui et al., 2013) and/or the formation of solid solutions in which Mn species are incorporated into the fluorite structure (Machida et al., 2000). It has been reported that when solid solutions are formed, the replacement of Ce^{4+} by Mn^{x+} could result in the contraction of the unit and the consequent shift of the diffraction peaks of CeO_2 to higher angles, since the radius of Mn^{x+} cation is smaller than that of Ce^{4+} (Zhan et al., 2014). However, this shift is not observed in Figure 5 and the formation of mixed oxide solid solutions cannot be confirmed for the prepared MnO_x-CeO_2 catalyst.

Apart from fluorite's characteristic peaks, two additional small peaks appear in the MnO_x-CeO_2 sample at 37.6º and 38.5º, corresponding to MnO_2 and Mn_2O_3 crystals, respectively. This fact suggests that small MnO_x crystals are present in the catalyst microstructure. The average crystallite size was calculated by the Scherrer equation, using the peaks that did not overlap. The results were 5.63 nm for MnO_2 crystals and 22.31 nm for Mn_2O_3 crystals, which confirmed that the crystallites are considerable. Previous works (Gallastegi-Villa, 2016; Tang et al., 2007) indicate that a large amount of MnOx crystals have a detrimental effect on catalytic activity. Therefore, probably higher operation temperatures will be necessary with the prepared MnO_x-CeO_2 catalyst than with highly amorphous catalysts.

4.1.3 Redox behavior

The results of H_2-TPR analyses for the MnO_x-CeO_2 sample and reference MnO_x and CeO_2 are represented in Figure 6. The profile of MnO_x-CeO_2 shows two overlapped reduction peaks at 289 and 323 ºC and a strong reduction peak at 424 ºC. Assuming that MnO is the final reduction state, it is generally accepted that the reduction of Mn species can be described by the successive process: $MnO_2/Mn_2O_3 \rightarrow Mn_3O_4 \rightarrow MnO$ (Dai et al., 2012; Gallastegi-Villa, 2016). When analyzing the reduction steps of different MnO_x samples, Kapteijn et al. (1994) observed that there was no clear reduction peak for an intermediate transformation of MnO_2 into Mn_2O_3, suggesting that this steps takes place very rapidly. These observations are in accordance with

the two overlapped low temperature peaks of the MnO_x-CeO_2 sample, which may correspond to MnO_2 and Mn_2O_3 reductions, successively. The high temperature reduction peak is attributed to Mn_3O_4 reduction.

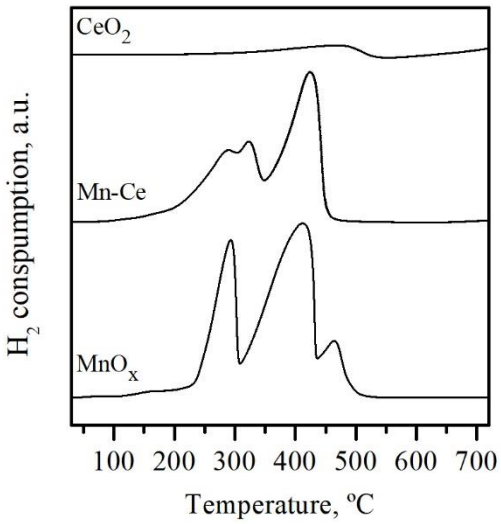

Figure 6. H_2-TPR profile of MnO_x-CeO_2 compared to reference MnO_x and CeO_2.

When comparing MnO_x-CeO_2 and reference MnO_x profiles, it has been reported in the literature that the peaks of the mixed oxide are shifted to lower temperatures (Wang et al., 2008; Gallastegi-Villa, 2016). This is attributed to the enhancement of oxygen mobility and hence the reducibility of the mixed oxide, when Mn ions are incorporated to the fluorite structure (Tang et al., 2006; Wu et al., 2008). In contrast, Figure 6 shows that the reduction peaks of the MnO_x-CeO_2 catalyst are shifted differently. The first overlapped peak at 290 ºC is shifted to lower temperatures, which may be related to Mn ions incorporated to the fluorite structure. The other two peaks are slightly shifted to higher temperatures, suggesting that part of MnO_x crystallites remained in their original state.

The average Mn oxidation state was estimated from the total hydrogen consumption. Assuming that the final oxidation state is Mn^{2+} and that hydrogen consumed by CeO_2 is negligible, it was concluded that 78.5% of Mn was in form of Mn^{3+} and the remaining 21.5% as Mn^{4+}.This result is accordance with XRD conclusions, since Mn_2O_3 was the most abundant crystal phase.

4.1.4 Acidic properties

NH_3-TPD results are represented in Figure 7. The profile is characteristic of metal oxide catalysts, showing fluctuations without big strongly defined peaks. Nonetheless, the profile exhibits a low temperature peak centered at 100 ºC, attributed to the desorption of NH_3 at weak acid sites. As temperature increases, the strength of acid sites leading to small desorption peaks in the profile also increases. Literature suggests that NH_4^+ ions anchored at Brønsted acid sites are less stable than NH_3 species at Lewis sites. Therefore, the low temperature desorption peak corresponds Brønsted sites, while at higher temperature Lewis sites would gain importance (Yao et al., 2017).

Time integration of the NH_3-TPD data revealed that, in total, 0.259 mmol NH_3 / g were desorbed in the process. This is a considerable amount, larger than some types of VO_x/TiO_2 catalysts (Gallastegi-Villa, 2016).

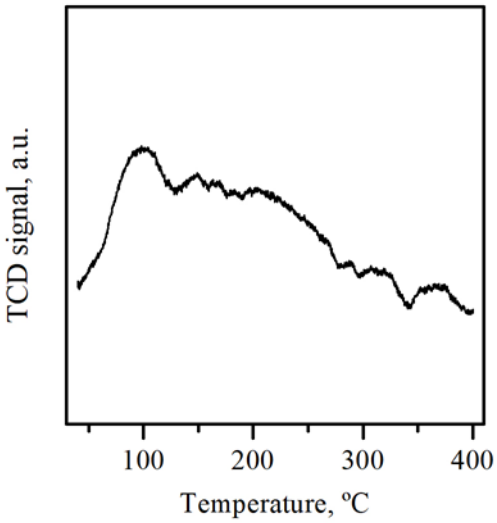

Figure 7. NH_3-TPD profile of MnO_x-CeO_2.

4.2 CATALYTIC ACTIVITY

4.2.1 MnO_x-CeO_2 as alternative to commercial VO_x/TiO_2 catalyst

The catalytic performance of the MnO_x-CeO_2 catalyst was monitored by determining the NO and o-DCB removal conversions as a function of temperature, under the conditions given in Table 3. The characteristic light-off curves are represented in Figure 8. It is important to point out that all conversions were measured at steady state, since the catalyst undergoes significant deactivation, as will be discussed later on.

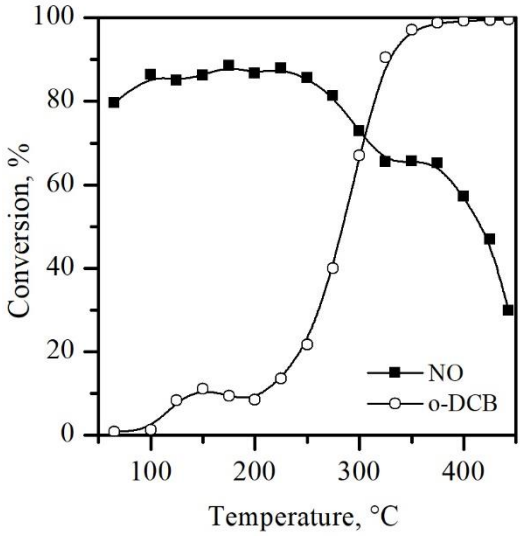

Figure 8. NO and o-DCB conversions in the simultaneous abatement over MnO_x-CeO_2.

NO reduction occurs at lower temperature than o-DCB oxidation, but both pollutants show conversions above 60% at the same temperature range, from 293 to 390 °C, indicating that the simultaneous abatement of NO_x and o-DCB is feasible. o-DCB conversion shows typical S shaped light-off achieving maximum conversion above 350 ºC, due to the exponential dependence of the reaction kinetic constant with temperature, described by the Arrhenius equation. Nonetheless, it has a low temperature peak, centered at 150 ºC. NO conversion should

also follow the S shape, but it reaches high conversions at temperatures as low as 65 ºC. This gives us an idea of the high oxidizing power of the catalyst, which could result in a better overall performance in the dDiNOx process. NO conversion profile shows two plateaus: a high conversion plateau (> 85%) from 100 to 250 ºC and a 65% conversion plateau from 325 to 375 ºC. At temperatures above 375 ºC NO conversion drops drastically.

In order to put these results in context, the performance of the alternative MnO_x-CeO_2 catalyst should be compared to that of the commercial catalyst VO_x/TiO_2. In Figure 9 the conversions of NO and o-DCB of the commercial VO_x/TiO_2 catalyst tested in the same experimental set-up and conditions are represented together with the conversions of the alternative MnO_x-CeO_2 (Gallastegi-Villa, 2016).

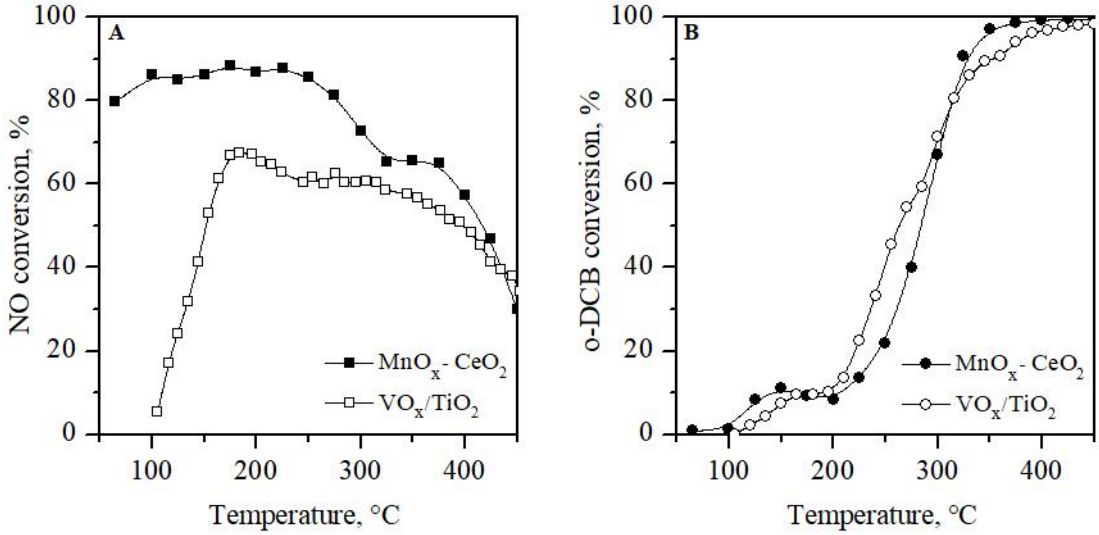

Figure 9. Comparison of the dDiNOx performance of MnO_x-CeO_2 and VO_x/TiO_2 in A) NO conversion and B) o-DCB conversion.

Figure 9A reveals that significantly higher NO conversions are obtained with MnO_x-CeO_2 than the commercial catalyst in the whole temperature range, especially at low temperatures. The alternative MnO_x-CeO_2 catalyst has a maximum conversion plateau at ca. 87%, while with VO_x/TiO_2 the NO conversion steadily decreases with temperature after reaching maximum conversion (ca. 68%). Above ca. 375 ºC, NO conversion declines dramatically in both catalysts due to parallel reactions, as will be extensively discussed later on.

Regarding o-DCB oxidation, both catalysts show a typical S shape behavior with similar oxidation temperatures (Figure 9B). The commercial catalyst shows higher conversions at the first stages of the oxidation, from 200 to 312 ºC, temperature at which both light-off curves cross. MnO_x-CeO_2 reaches maximum conversion at lower temperatures. It should be pointed out that at such high temperatures molecule diffusion processes may be controlling the overall process, since the average pore size is smaller in MnO_x-CeO_2 than VO_x/TiO_2 (6 nm vs. 10 nm). The mixed oxide formed in MnO_x-CeO_2 was expected to oxidize o-DCB at significantly lower temperatures, and therefore, it looks like only a small part of the catalyst had the desired mixed oxide structure. This is in accordance with the conclusions drawn from XRD and H_2-TPR results, where crystalline species and low reducibility of the catalyst were observed.

The biggest challenge of the combined abatement of NO_x and PCDD/Fs is to remove completely and selectively both pollutants in the same temperature range. Hence, in terms of conversion, a

faster o-DCB oxidation reaction is required, maintaining high NO conversion. For the sake of this research, the working temperature window was defined as the temperature range at which the conversion of pollutants, is higher than 60%. Same criteria as Gallastegi-Villa (2016) was followed. Thus, based on Figure 8, the working window for MnO_x-CeO_2 catalyst is from 293 to 390 °C, at the specific conditions of this experiment. This is a much wider range than the commercial VO_x/TiO_2 catalyst, which was determined to be from 285 to 330 ºC. This is a big point in favor of the presented alternative catalyst, since it will exhibit a more reliable and robust behavior in real life applications.

In order to determine whether pollutants are removed selectively or not, product formation profiles were monitored in the above experiment and they are represented in Figure 10.

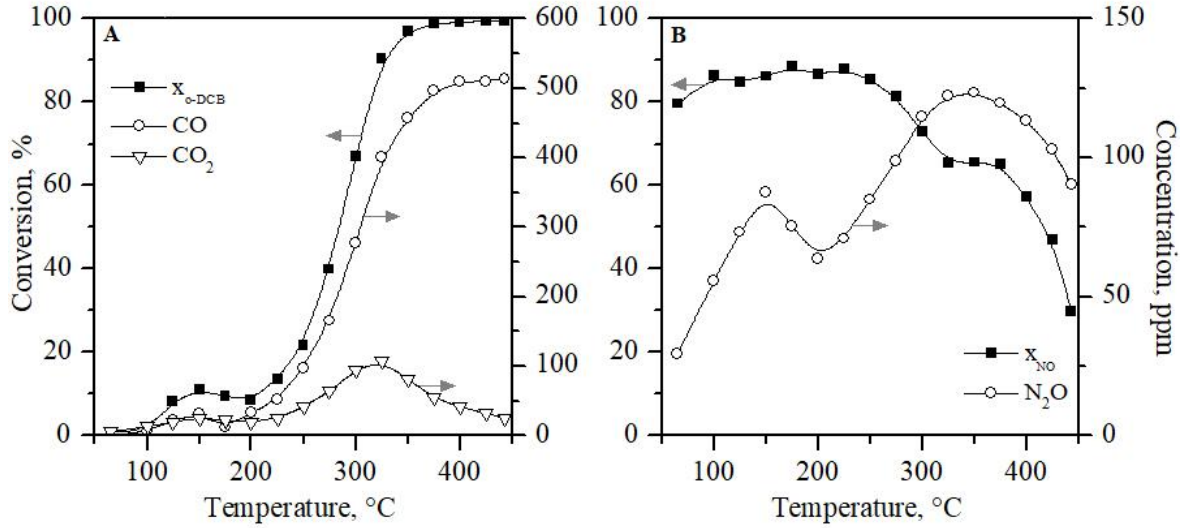

Figure 10. Reactant conversion and product formation profiles in the dDiNOx process for A) NO reduction and B) o-DCB oxidation over MnO_x-CeO_2.

Figure 10A shows that o-DCB oxidation tends to complete oxidation, since considerable CO_2 amounts are measured at the outlet of the reactor, larger than CO at all temperatures. However, there is a CO formation peak at 325 ºC, temperature at which o-DCB conversion almost reaches its maximum. Further increase of temperature results in higher selectivity towards CO_2. Significantly more CO is produced over the commercial catalyst, with a maximum of ca. 245 ppm at 450 ºC (Gallastegi-Villa, 2016), evidencing the better oxidizing behavior of MnO_x-CeO_2. The formation of oxidation byproducts should be also considered, since they may affect the selectivity significantly. Over MnO_x-CeO_2 only trace amounts of chlorinated byproducts were detected from 225 ºC to 375 ºC: trichloronitromethane, tetrachloroethylene and trichlorobenzenes. In contrast, using the commercial VO_x/TiO_2 catalyst DCMA was formed, and up to 15 ppm were detected in the middle temperature range, between 225 ºC and 400 ºC.

A carbon balance was carried out for the results obtained with MnO_x-CeO_2, represented in Figure 11. In this figure, 'Ads + Byp' represents the sum of the amount of o-DCB adsorbed in the catalyst and the generated byproducts (trichloronitromethane, tetrachloroethylene and trichlorobenzenes). This amount was calculated considering the carbon necessary to close the carbon balance. Figure 11 evidences that a significant amount of o-DCB was adsorbed in the catalyst, especially at low temperatures, representing up to 35% of total carbon at 175 ºC. The increased selectivity towards CO_2 with temperature is also evidenced.

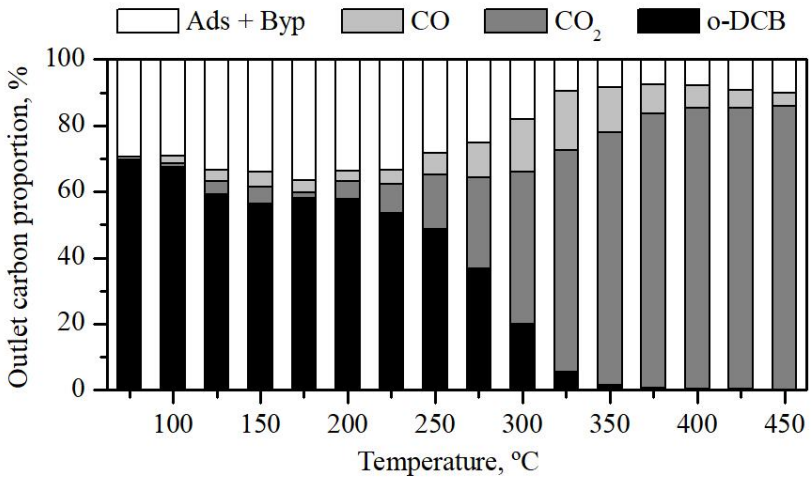

Figure 11. Carbon balance of the dDiNOx process over MnO_x-CeO_2.

On the other hand, Figure 10B reveals that significant N_2O production takes place throughout the dDiNOx process over MnO_x-CeO_2. A rather unique N_2O formation curve is observed, due to the complexity of the process with various competitive reactions, as will be discussed later on. At this point, it should be mentioned that using the commercial VO_x/TiO_2 catalyst in the same experimental set-up and conditions, N_2O only forms above 300 ºC, with a typical S shape curve (Gallastegi-Villa, 2016).

Besides high activity and selectivity, catalysts need to have high durability in the catalysis environment in order to be suitable for a real life application. Figure 12 shows the stability test of MnO_x-CeO_2 catalyst carried out during 44 h of time-on-stream at 300 ºC.

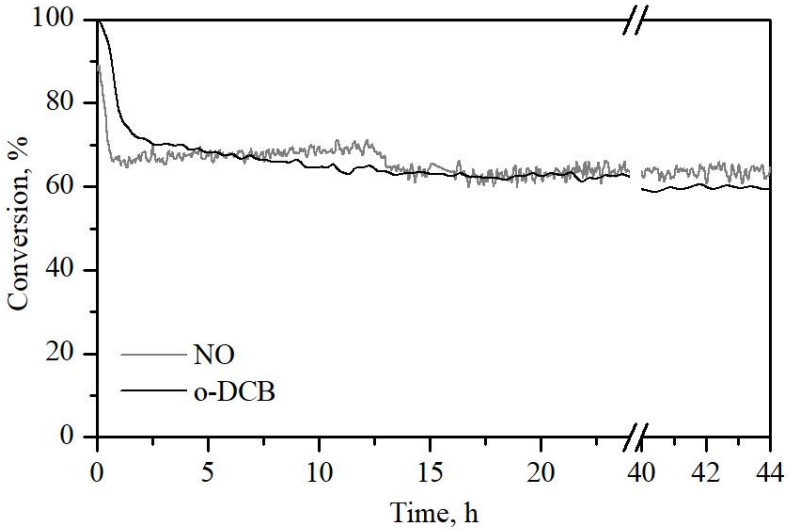

Figure 12. Durability test of MnO_x-CeO_2 in the dDiNOx process at 300 ºC.

It can be observed in Figure 12 that deactivation of the catalyst is noticeable. NO conversion drops from 90 to ca. 65% in the first hour, but it is stable all along the test at ca 65%. The slight fluctuations can be attributed to experimental limitations. On the other hand, within the first 2 hours, o-DCB conversion drops from 100% to ca. 70%, due to a partial deactivation of the catalyst. The initial conversion drops of both pollutants are very likely because of the blockage

of active sites by the adsorbed chlorine atoms produced from the decomposition of o-DCB (Wang et al., 2008). Apart from the initial drop, o-DCB conversion has a slight reduction tendency, and it is finally stabilized at ca. 60% after 44 h. This type of deactivation was also observed by Wang et al. (2008) over MnO_x-CeO_2 mixed oxide catalyst with different manganese loadings. There are discrepancies in the literature when it comes to the origin of the deactivation. Wang et al. (2008) proposed that the deactivation of catalysts during the combustion of chlorobenzene is related to the poisoning of Ce species, since the level of activity drop was parallel to the amount of Ce species in the catalyst. However, it has been proved that the manganese phase also undergoes deactivation (Gallastegi-Villa, 2016). So, considering that the catalyst is a mixture of metals with strong interactions between them, deactivation probably occurs in both metals, but it may be more severe for the Ce phase.

In order to be able to use the catalyst in a real-life application, it is essential to analyze the effect of H_2O in the process, since 10-20% in volume should be expected in the combustion chamber outlet. However, at these concentrations water is in excess and, apart from causing experimental difficulties, it would be difficult to analyze its effect on reaction kinetics. So, it was decided to work with a maximum concentration of 1%, in which water is also in excess but its effect would be noticeable. Experiments were carried out with step feeds of H_2O (0-0.5%) during the dDiNOx process at 150 ºC and 300 ºC, represented in Figure 13.

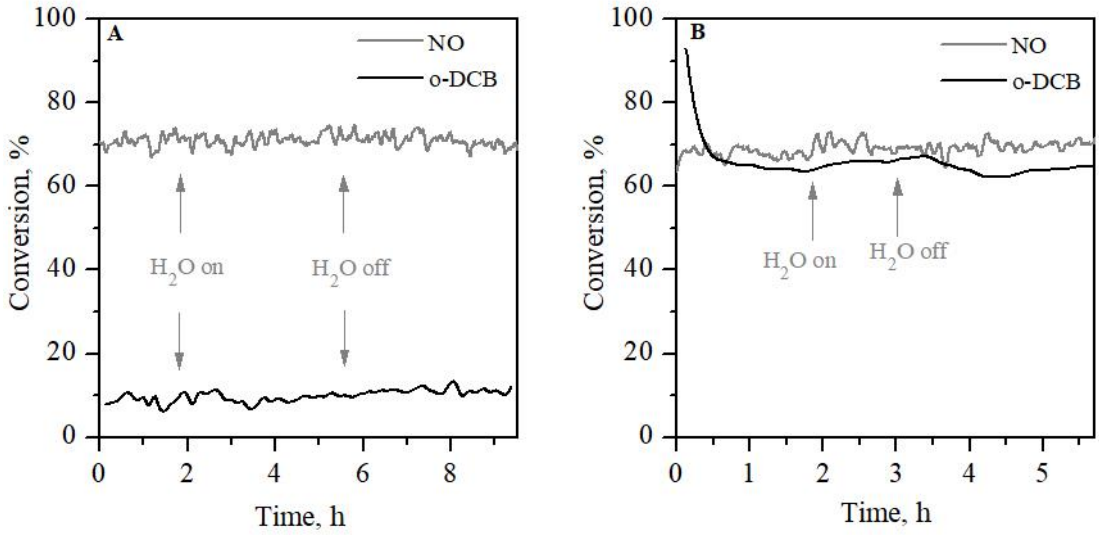

Figure 13. Step feeds of water (0-0.5%) during the dDiNOx process over MnO_x-CeO_2 at A) 150 ºC and B) 300 ºC.

Figure 13 reveals that the effect of water in the dDiNOx process over MnO_x-CeO_2 is negligible. At 150 ºC, the presence of water does not vary neither o-DCB nor NO conversion. At 300 ºC, a slight o-DCB conversion increment is observed when water is fed. However, when water is not fed the conversion does not drop immediately and these variations may be due to experimental limitations, since they are within the range of experimental error. The selectivity of the process does not significantly vary with the presence of water at both temperatures. An additional experiment was carried out with a step feed of water (0-1%) at 300 ºC, and the same results were obtained, water did not vary significantly any reactant conversion or product production. This result confirms that the absence of any effect observed in Figure 13 is not due to low water concentration.

In contrast, water has a considerable effect on the conversions of both pollutants over the commercial VO_x/TiO_2 catalyst. In previous studies by TQSA group, it was observed that when water was fed, NO conversion decreased significantly in the temperature range where SCR reaction was predominant (below 150 ºC), due to the competitive adsorption of H_2O and NH_3 in Brønsted sites. For the same reasons, the presence of water also led to a decrease of o-DCB conversions above 300 ºC, but, in contrast, it had a promotional effect at low temperatures. The promotion was attributed to the removal of adsorbed Cl and reaction intermediates from the active sites. So, the fact that water does not influence the dDiNOx process is another important advantage of the alternative MnO_x-CeO_2 catalyst, since its behavior will be more reliable and predictable in real life applications.

4.2.2 Identification of side reactions

NO reduction reactions with NH_3 have been studied for decades and the investigation has shown that many side reactions take place in parallel. These reactions may have a significant impact in the performance and selectivity of the process and it is, therefore, essential to identify them. In fact, it can be observed in Figure 10 that SCR and CTO reactions are not completely selective, showing the formation of unwanted products such as CO and N_2O. Furthermore, the NO conversion drop at high temperature is probably caused by side reactions. In this section an attempt was made to determine the most prominent reactions.

The unusual N_2O formation curve observed in Figure 10B may give some clues to the side reactions occurring during the dDiNOx process. According to literature, various side reactions may be the origin of N_2O. A non-selective SCR has been observed to take place over mixed oxide catalysts (Lietti et al., 2000; Brandenberger et al., 2008), leading to the formation of unwanted N_2O.

$$4\ NH_3 + 4\ NO + 3O_2 \rightarrow 4\ N_2O + 6\ H_2O \quad (7)$$

In addition, instead of reacting through SCR, NH_3 may oxidize by O_2 to N_2O, according to equation (8).

$$2\ NH_3 + 2\ O_2 \rightarrow N_2O + 3\ H_2O \quad (8)$$

NO may also consume by its decomposition and disproportionation reactions giving rise to N_2O, according to equations (9) and (10), respectively.

$$2\ NO \rightarrow N_2O + 1/2\ O_2 \quad (9)$$

$$3\ NO \rightarrow N_2O + NO_2 \quad (10)$$

In order to determine which reactions are preferentially taking place in the process, subsequent experiments of NH_3 oxidation and NO oxidation were carried out, represented in Figure 14 and Figure 15, respectively. In these reactions, it was vital to measure NH_3 and NO_2 concentrations; and therefore, they were performed in an alternative reactor connected on-line to an FT-IR gas analyzer (MKS FT-IR Multigas Analyzer 2030), which can measure the concentration of any compound except diatomic molecules.

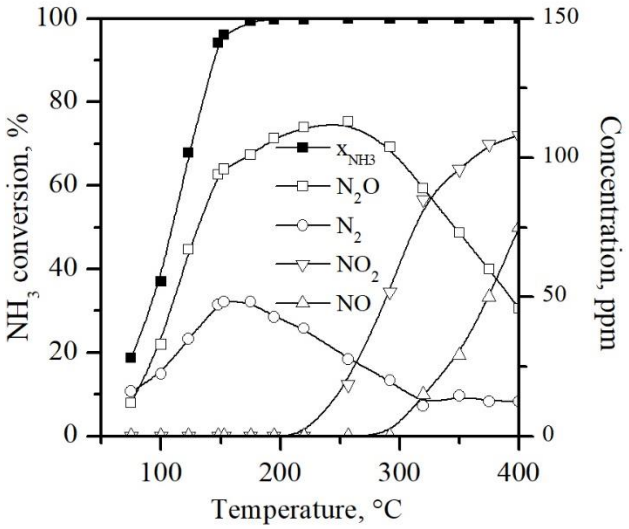

Figure 14. NH_3 conversion and N_2O, N_2, NO_2 and NO formation in NH_3 oxidation reaction over MnO_x-CeO_2.

Figure 14 shows NH_3 conversion when 300 ppm NH_3 and 10% O_2 were fed to the catalytic reactor, with the reaction conditions given in Table 3. Total NH_3 conversion is reached as low as 175 ºC, showing, the oxidizing power of the prepared catalyst. According to literature, apart from Equation (8), NH_3 may oxidize by O_2 to N_2 (selective oxidation) and NO, according to Equation (11) and Equation (12), respectively. The produced N_2 was determined by nitrogen balance.

$$4\ NH_3 + 5\ O_2 \rightarrow 4\ NO + 6\ H_2O \quad (11)$$

$$4\ NH_3 + 3\ O_2 \rightarrow 2\ N_2 + 6\ H_2O \quad (12)$$

The main product of NH_3 oxidation is the unwanted N_2O, formed according to Equation (8), showing that part of N_2O detected in the dDiNOx process probably arises from NH_3 oxidation. Above 200 ºC, NO_2 and NO are detected and their concentration increases sharply at higher temperatures. NO is formed according to Equation (11) and part of it is subsequently oxidized to NO_2, according to Equation (13).

$$NO + 1/2\ O_2 \rightarrow NO_2 \quad (13)$$

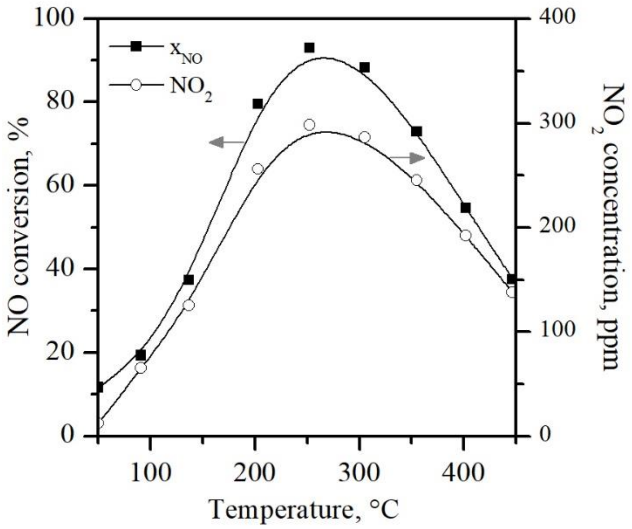

Figure 15. NO conversion and NO_2 formation in NO oxidation reaction over MnO_x-CeO_2.

In Figure 15 NO conversion is represented when 300 ppm NO and 10% O_2 were fed to the catalytic reactor, with the reaction conditions given in Table 3. NO conversion and NO_2 formation increase sharply with temperature up to 250 ºC, temperature at which maximum conversion is reached (93%). Above this temperature NO conversion decreases, forming, consequently, less NO_2. Only trace amounts of N_2O were detected, indicating that NO decomposition (Equation (9)) and disproportionation (Equation (10)) reactions are insignificant over MnO_x-CeO_2. Thus, it can be concluded that N_2O formation, in the dDiNOx process preferentially arises from NH_3 oxidation reaction (Equation (8)) and/or from the non-selective SCR reaction, given in Equation (7).

Both oxidation reactions confirm the higher oxidation power of MnO_x-CeO_2 than commercial VO_x/TiO_2. In NH_3 oxidation, only ca. 20% NH_3 conversion was obtained at 470 ºC over VO_x/TiO_2. However, no N_2O formation was observed and its selectivity towards N_2 was 100% (Gallastegi-Villa, 2016). Regarding NO oxidation, maximum conversion was reached at much higher temperatures (ca. 460 ºC) with VO_x/TiO_2 (ca. 460 ºC).

4.2.3 Insight into reaction pathways

Thus far, the potential of MnO_x-CeO_2 catalyst as an alternative to commercial VO_x/TiO_2 has been proven. The performed reactions have shown the complexity of the process with various side reactions taking place simultaneously. Additionally, at this point, it is unknown if both reaction have interactions altering the abatement efficiency, as observed in VO_x/TiO_2. In order to be able to predict the behavior of the catalyst in different environments and ensure its reproducibility, it is essential to understand the mechanisms through which the reactions are taking place.

Based on the present investigation as well as earlier reports (Marbán et al., 2004; Eigenmann et al., 2006; Xu et al., 2013; Qi et al., 2004), the SCR reaction of NO by NH_3 over MnO_x-CeO_2 most probably proceeds via a combination of ER and LH mechanisms.

In a typical ER mechanism, NH_3 is first adsorbed in Lewis acid centers forming intermediates like NH_2^-, which consequently react with gas phase NO and NO_2 (• represents a Lewis acid site on the surface of the catalyst).

$$NH_3 + \bullet \leftrightarrows NH_2^- \bullet + H \quad (15)$$

$$NH_2^- \bullet + NO \rightarrow N_2 + H_2O \quad (16)$$

On the other hand, two adsorbed species participate in reactions following LH mechanism. This mechanism requires more steps and different pathways have been proposed in the literature. Based on FT-IR studies, Qi et al. (2004) proposed an amide-nitrosoamide type mechanisms for SCR of NO over manganese-cerium oxides.

$$O_2\,(g) \rightarrow 2\,O \quad (17)$$

$$NH_3\,(g) \rightarrow NH_3\,(a) \quad (18)$$

$$NH_3\,(a) + O\,(a) \rightarrow NH_2\,(a) + OH\,(a) \quad (19)$$

$$NO\,(g) + 1/2\,O_2\,(g) \rightarrow NO_2\,(a) \quad (20)$$

$$NH_2\,(a) + NO\,(g) \rightarrow NH_2NO\,(a) \rightarrow N_2\,(g) + H_2O\,(g) \quad (21)$$

$$OH\,(a) + NO_2\,(a) \rightarrow O\,(a) + NH_2NO\,(a) + H_2O \rightarrow N_2\,(g) + 2\,H_2O\,(g) \quad (22)$$

They observed that at high temperature N_2O was produced by the reaction of NH_3 with nitrate. It is important to point out that, in this mechanism, various species are adsorbed in different Lewis and Brønsted acid sites.

In order for both mechanisms to proceed, the adsorption of NH_3 on the catalyst is a necessary step. NH_3 may be adsorbed in the two types of acid sites present in MnO_x-CeO_2. Many publications suggest that NH_3 adsorbed in Lewis sites is very important for low-temperature SCR (Wu et al., 2007a; Li et al., 2007), while Brønsted sites prevail at higher temperatures (Topsoe et al., 1995). Consequently, it is expected that as temperature increases the predominant mechanisms will shift from ER to LH.

Regarding o-DCB oxidation mechanisms, it has been proposed that chlorobenzene oxidation over metal oxide catalysts follows a MVK mechanism (Dai et al., 2012; Sun et al., 2016). The mechanism consists of the adsorption of chlorobenzene in Brønsted acid sites and subsequent oxidation by lattice oxygen involving ring-opening reactions. At this point, it is evident that competence between SCR LH reaction and o-DCB oxidation through MVK mechanism may exist, since both involve reactant adsorption in Brønsted sites. In addition, o-DCB oxidation has also been reported to follow a simpler reaction pathway: dechlorination of o-DCB into benzene which may then oxidize by chemisorbed oxygen species into CO, CO_2 and H_2O (Sun et al., 2016). The activity of surface oxygen plays a key role in this mechanism, and in this regard, the presence of NO_2 demonstrated in Figure 15 may have an important role to play. This is because researches have repeatedly proved that the presence of NO_2 promotes the formation of surface oxygen species more active than only in the presence of O_2, enhancing the oxidation potential of metal oxide catalysts (Centi et al., 2001; Kondratenko et al., 2007; Gallastegi-Villa, 2016).

In order to clarify the complex nature of the dDiNOx process and be able to propose a suitable scheme, experiments carried out in different conditions are compared. So as to identify if interactions between NO reduction and o-DCB oxidations exist, in Figure 16 the simultaneous (S) and independent (I) abatement of o-DCB are compared. The following were the reaction conditions of the independent o-DCB oxidation: 100 ppm o-DCB, 10% O_2 and balance Ar (2 L_N/min, 80000 h^{-1}).

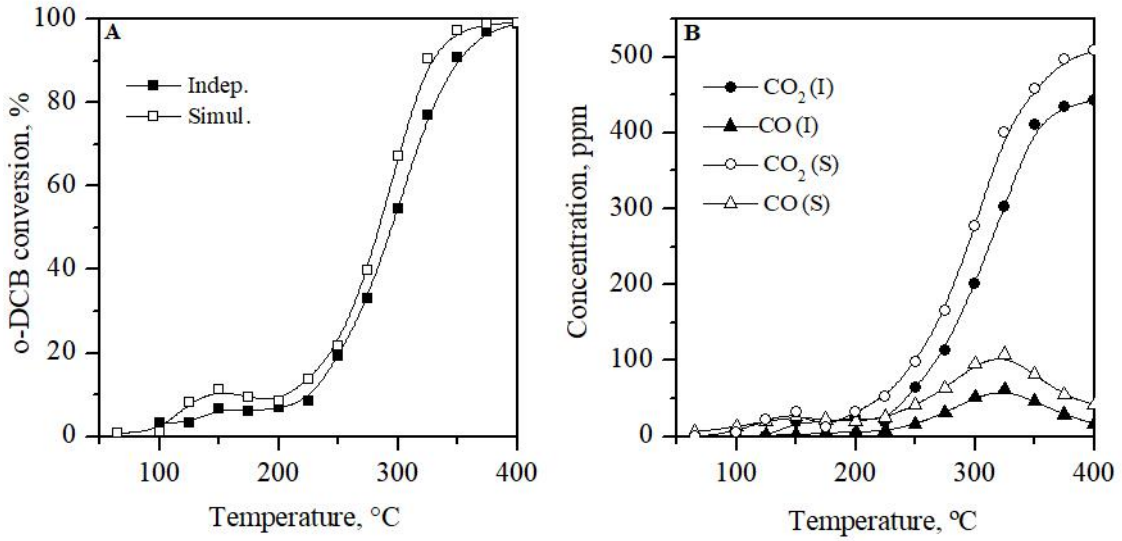

Figure 16. Comparison of A) o-DCB conversion and B) CO and CO_2 formation in the independent (I) and simultaneous (S) abatement over MnO_x-CeO_2.

Figure 16 reveals that o-DCB conversion is slightly higher in the simultaneous dDiNOx process than in the independent o-DCB oxidation reaction. Nonetheless, the curves represented in Figure 16A are too similar to confirm that there is any effect of NO and NH_3 co-feeding on o-DCB oxidation activity. Under both conditions, two different temperature zones can be distinguished. The low temperature conversion peak may me associated to the simple dechlorination mechanism. As temperature increases, o-DCB molecules start to be adsorbed in Brønsted sites, but until 200 ºC not enough energy is provided to activate the reaction. Above this temperature, standard o-DCB oxidation reaction occurs via MVK mechanism, increasing the conversion drastically.

The absence of a notable effect suggests that the promotional effect of NO associated to NO_2 and attributed to its higher oxidation potential than O_2 (Centi et al., 2001; Kondratenko et al., 2007; Gallastegi-Villa, 2016) is negligible over MnO_x-CeO_2. This fact may be because the kinetically significant step is not associated to surface oxygen species, in contrast to VO_x/TiO_2. MnO_x-CeO_2 high oxygen mobility facilitates the activation of oxidation reactions and replaces oxygen vacancies efficiently.

On the other hand, over VO_x/TiO_2 competition between o-DCB and NH_3 for the same acid sides was confirmed, which reduced o-DCB conversion above 250 ºC (Gallastegi-Villa, 2016). In case of MnO_x-CeO_2 the absence of an effect of NH_3 on o-DCB conversion suggest that, even though competition may exist, o-DCB is preferentially adsorbed in Brønsted acid sites.

With the purpose of identifying the influence of the concentration of SCR gases on o-DCB oxidation, the conversions and product concentrations at different NO and NH_3 concentrations are represented in Figure 17, at 150 ºC and 300 ºC. Although a slight promotional effect is observed when 300 ppm of NO and NH_3 were fed, at higher concentrations o-DCB conversion drops again (Figure 17A). Product formation profiles have similar shapes, but it is noteworthy that a slight reduction of selectivity towards CO_2 is observed when 600 ppm of NO and NH_3 were fed. However, a big impact was noted on the byproduct production when NH_3 was present. In order to evaluate this effect and elucidate the role of NO, an additional experiment was carried out with step feeds of NO (0-300 ppm) and NH_3 (0-600 ppm) during o-DCB oxidation at 300 ºC, represented in Figure 18.

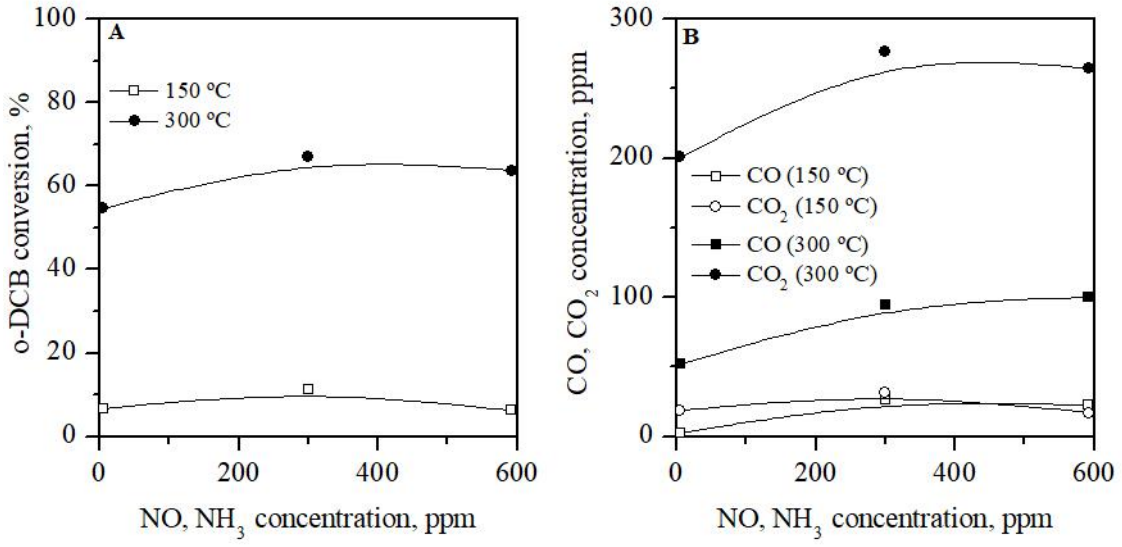

Figure 17. Effect of NO and NH_3 inlet concentrations in A) o-DCB conversion and B) CO and CO_2 formation over MnO_x-CeO_2.

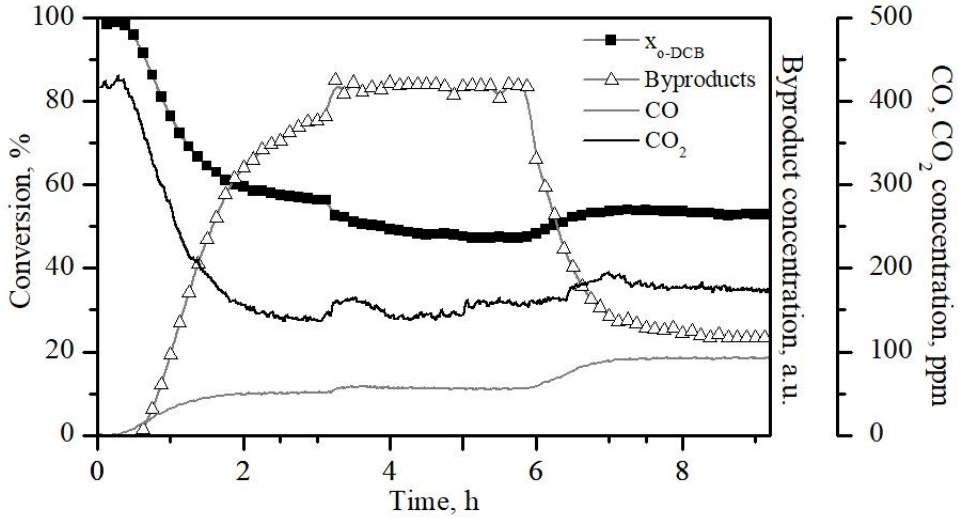

Figure 18. Transient o-DCB oxidation reaction with step feeds of NO (0-300 ppm) and NH_3 (0-600 ppm) at 300 ºC over MnO_x-CeO_2.

It is observed in Figure 18 that when the NO is injected, o-DCB conversion slightly reduces, confirming that the promotional effect related to NO_2 is inexistent. The slight conversion reduction may be explained by the competence of NO and o-DCB for Brønsted sites. In contrast, when NH_3 is injected, the slight promotional effect observed in Figure 16A is repeated, which may be attributed to the change in acidity of the catalyst. This may promote the complex MVK reaction pathways. Nevertheless, NH_3 impacts most significantly the selectivity of o-DCB oxidation, since total byproduct formation is reduced almost to a quarter (detected by GC_MS). CO and CO_2 formation increase when NH_3 is injected, according to the increase in o-DCB conversion. This indicates that the aromatic ring of o-DCB was cracked more effectively in the presence of NH_3. In addition, NH_3 may also react with surface chlorine atoms produced in o-DCB oxidation, to form NH_4Cl, reported to take place over mixed the commercial VO_x/TiO_2 catalyst (Gallastegi-Villa, 2016; Hou et al., 2014). This reaction may wash out the accumulated chlorine from the active sites of MnO_x-CeO_2, retaining its oxidizing capacities. A similar effect

was observed by Sun et al. (2016) with the presence of water in o-DCB oxidation over MnO_x-CeO_2.

A comparison of the simultaneous (S) and independent (I) abatement of NO was also carried out. The following were the reaction conditions of the independent NO reduction: 300 ppm NO, 300 ppm NH_3, 10% O_2 and balance Ar (2 L_N/min, 80000 h^{-1}).

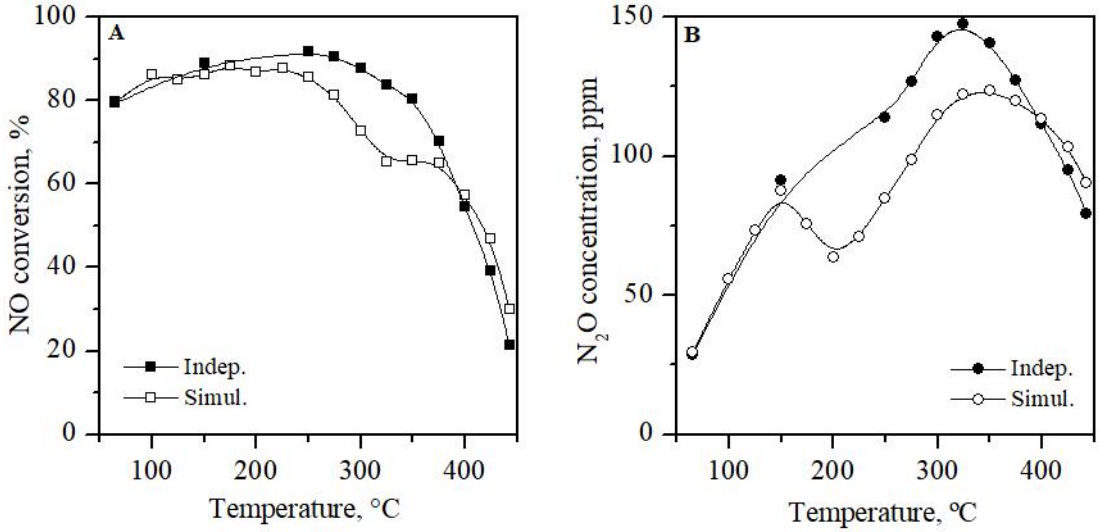

Figure 19. Comparison of A) NO conversion and B) N_2O formation in the simultaneous and independent abatement over MnO_x-CeO_2.

Figure 19A shows that at low temperatures NO conversion is unaffected by the presence of o-DCB. But, between 200 ºC and 395 ºC, SCR activity is reduced in the simultaneous dDiNOx process, causing, at most, a 19% NO conversion drop. This fact confirms the competitive adsorption of o-DCB, NO and NH_3 in Brønsted acid sites, and it can be concluded that o-DCB adsorption inhibits SCR LH mechanism. Over VO_x/TiO_2 catalyst, the reduction of NO conversion in the presence of o-DCB was also observed, but this happened at the whole temperature range (Gallastegi-Villa, 2016).

A comparison of experiments with different feeding o-DCB concentration (Figure 20) reveals that the inhibition effect is related to the amount of o-DCB in the catalyst, since lower NO conversions are obtained with increasing o-DCB concentration. In this figure, N_2O concentration reduces according to the decrease of NO conversion.

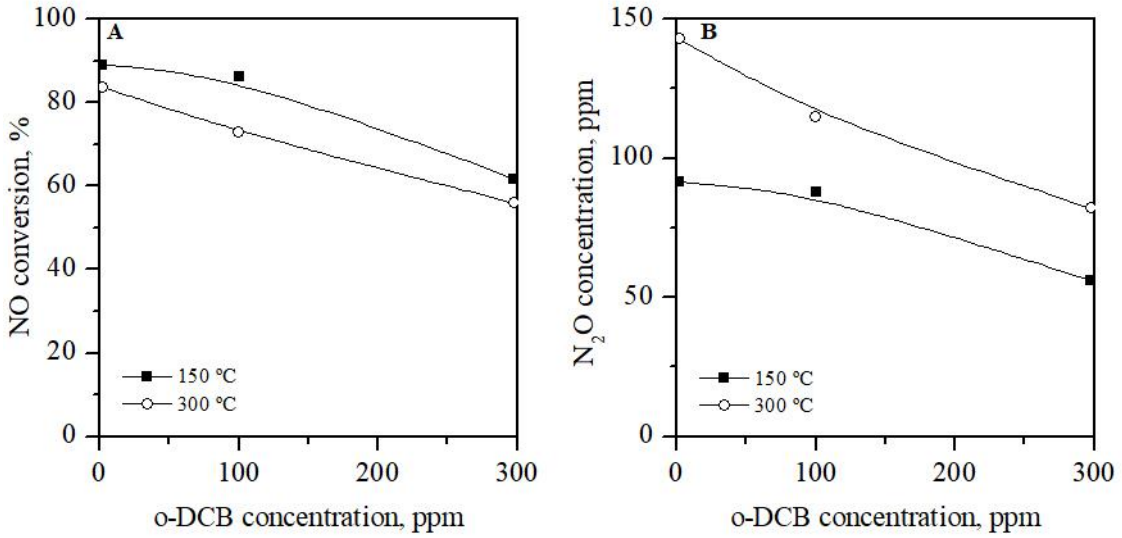

Figure 20. Effect o-DCB inlet concentration in A) NO conversion and B) N_2O formation over MnO_x-CeO_2.

The decrease of NO conversion due to the presence of o-DCB has an impact on N_2O formation (Figure 19B). But, very interestingly, the N_2O formation drop takes place between 150 ºC and 200 ºC. At this temperature range, it has been proposed that NO reduction follows preferentially the LH mechanism, but, when o-DCB is also adsorbed in Brønsted sites, this mechanism is inhibited. The fact that the inhibition due to adsorbed o-DCB and N_2O formation drop occur in the same temperature range suggests that the non-selective SCR reaction follows the LH mechanism. N_2O is probably formed due to the reaction of NH_3 with nitrate species (Qi et al., 2004).

Considering all the above mentioned, it is proposed that at low temperatures SCR reaction follows preferentially a ER mechanism, with high N_2 selectivity. As temperature increases, LH mechanism gains importance, producing more N_2O. This is evidenced with the N_2O formation drop at 150 ºC. At this temperature, o-DCB is adsorbed at Brønsted sites, reducing the number of available sites for the LH mechanism, and therefore reducing N_2O production.

It is noteworthy that due to the o-DCB inhibition effect the working temperature window (temperature range where both pollutants conversion is higher than 60%) is broader for the alternative MnO_x-CeO_2 than for VO_x/TiO_2. The fact that the inhibition effect does not affect the working temperature window is another clear advantage of the alternative MnO_x-CeO_2.

At this point, the only unresolved issue is to determine the origin of N_2O at different temperatures. As explained before, N_2O may arise from two reactions: non-selective SCR (Equation (7)) and NH_3 oxidation (Equation (8)). In Figure 21 two curves were drawn corresponding to fittings of the N_2O formation profile to the two reactions from which N_2O may arise, together with N_2O formation profiles in the independent and simultaneous reactions.

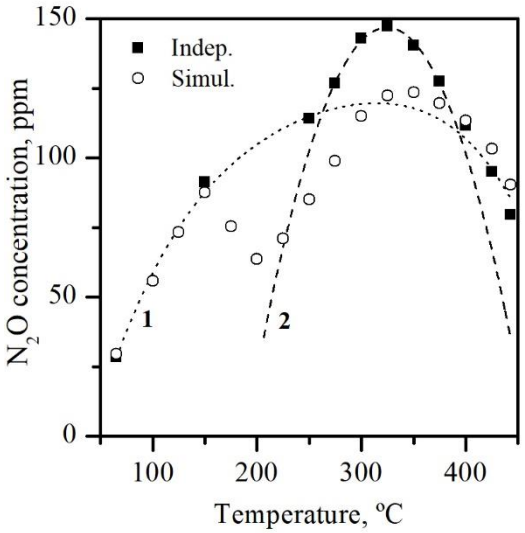

Figure 21. N_2O formation profiles and illustrative peaks corresponding to N_2O forming reactions in the simultaneous and independent abatement over MnO_x-CeO_2.

In the independent reaction, a broad N_2O concentration peak is observed, which corresponds to a N_2O formation reaction taking place at the whole temperature range (curve 1 in Figure 21**)**. The curve is disturbed with a narrower peak with maximum N_2O production at 325 ºC (curve 2 in Figure 21**)**. This peak would be explained by a N_2O formation reaction taking place only at high temperatures.

In order to determine which reaction (NH_3 oxidation or non-selective SCR) corresponds to each peak, it was considered that in the non-selective SCR given in Equation (7) NO and N_2O are directly related with a 1:1 stoichiometric relationship. Therefore, time dependent data collected during the reactions was analyzed (Figure 22), revealing that non-selective SCR is the origin of N_2O at low temperatures, since N_2O formation profile and NO conversion follow the same exact trends. An example of this is given in Figure 22A, where the same fluctuations are observed in both profiles at 125 ºC. This immediate dependence is not observed above 150 ºC. For instance, it can be seen in Figure 22B that at 250 ºC, N_2O concentration has an increasing tendency while NO conversion is constant. Considering these observations, it can be concluded that the non-selective SCR reaction (Equation (12)) takes place at the whole temperature range as represented in curve 1 in Figure 21, while NH_3 oxidation (Equation (8)) is the origin of the high temperature N_2O formation peak (curve 2 in Figure 21).

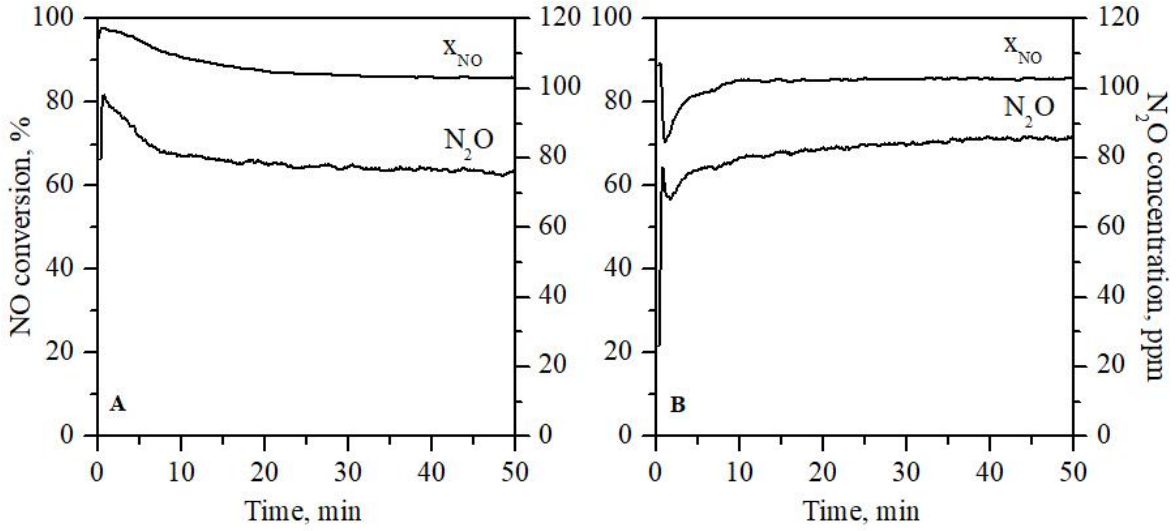

Figure 22. Time dependent NO conversion and N_2O concentration collected during the dDiNOx process at A) 125 ºC and B) 250 ºC.

To finish, in order to facilitate the interpretation of the results and propose a reaction scheme, reactant conversion and product concentration profiles of the dDiNOx process over the alternative catalyst MnO_x-CeO_2 have been separated in four temperature zones, as represented in Figure 23.

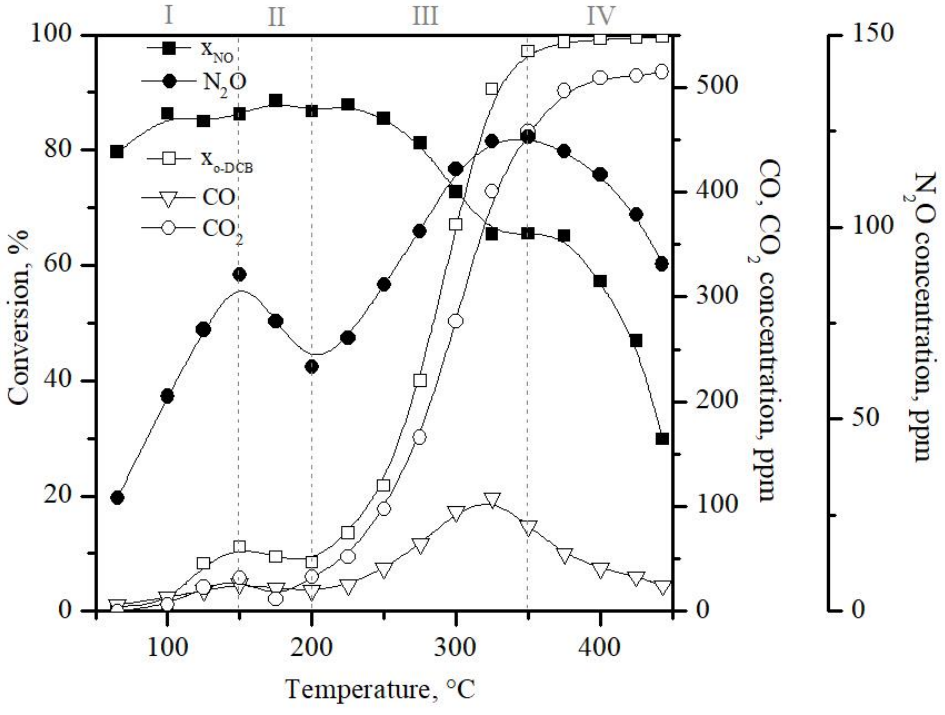

Figure 23. Reactant conversion and product formation profiles in the simultaneous abatement over MnO_x-CeO_2.

Based on our results and knowledge gathered in the literature, the dDiNOx conversion and product formation profiles divided in four zones (Figure 23) could be explained as follows:

I) In the low temperature range (zone I) the SCR reaction is unaffected by o-DCB. NO conversion reaches the maximum conversion plateau and N_2O concentration increases with temperature, as the LH mechanism gains importance over ER. o-DCB oxidation most probably follows the dechlorination mechanism, increasing the conversion with temperature up to ca. 10%.

II) In zone II, o-DCB starts to be adsorbed in Brønsted acid sites but the temperature is still too low to activate the MVK mechanism. Less Brønsted sites are available for SCR reaction to follow the LH mechanism, reducing N_2O formation. High NO conversion is maintained by the ER mechanism, which is not inhibited by o-DCB since only requires Lewis acid sites.

III) In the mid temperature range (zone III), NO conversion drops from ca. 85% to the high temperature plateau (65%). This drop is attributed to the increasing lack of Brønsted sites for the LH mechanism, and to NH_3 oxidation side reaction consuming part of available NH_3. Outlet N_2O concentration increases significantly up to ca. 123 ppm due to NH_3 oxidation reaction occurring according to Equation (8). On the other hand, o-DCB conversion increases sharply until nearly total conversion is achieved at 350 ºC. This reaction occurs via MVK mechanism and significant amounts of unwanted CO are produced until it reaches a maximum of 108 ppm at 325 ºC.

IV) At high temperatures (zone IV), NO conversion is initially maintained at 65% (high temperature plateau, 325 - 375 ºC). This plateau is explained by the competitive side reactions occurring simultaneously, since it coincides with a N_2O formation peak, justified by the shift of NH_3 oxidation reaction from Equation (8) forming N_2O to Equation (11) forming NO. Above 375 ºC, NO conversion drops drastically, probably due to the excess of NO formed in NH_3 oxidation, according to Equation (8). Regarding o-DCB oxidation, total conversions are maintained and the reduction of CO formation implies that at such high temperatures complete oxidation towards CO_2 is achieved.

5 CONCLUSIONS AND FUTURE WORK

Regarding the proposed objectives, the following conclusions can be drawn from the present research work.

- The simultaneous abatement of NO and o-DCB is feasible over the alternative catalyst MnO_x-CeO_2. Conversions of both pollutants over 60% are achieved at medium temperature (290-390 ºC), which is much broader range than the one of commercial VO_x/TiO_2. However, the initially expected improvement of activity at low temperature was not achieved, probably because the desired mixed oxide structure was not completely formed. The conversions of both pollutants are stable in the long term, even though partial chlorine deactivation is observed within the first two hours of catalytic tests. Moreover, unlike VO_x/TiO_2, the presence of water does not affect conversions and selectivity over MnO_x-CeO_2. The only downside of MnO_x-CeO_2 is that more unwanted N_2O is produced than over VO_x/TiO_2, most likely due to the non-selective SCR reaction at low temperature, while the oxidation of NH_3 towards N_2O is also considerable at high temperature.

- The characterization of the catalyst showed that the desired mixed oxide structure where Mn ions are incorporated to the Ce lattice was only formed partially. This was confirmed with the considerable Mn crystals detected in the XRD analysis and the absence of shifts of the peaks in XRD and H_2-TPR. The low reducibility of the catalyst explains the low o-DCB oxidation activity at low temperature.

- It can be concluded from NO and NH_3 oxidation reactions that the prepared MnO_x-CeO_2 catalyst is highly oxidizing, much more than VO_x/TiO_2. These tests also revealed that most N_2O detected in the dDiNOx process arises from the non-selective SCR reaction (Equation (7)) and oxidation of NH_3 towards N_2O (Equation (8)), since NO decomposition (Equation (9)) and disproportionation (Equation (10)) reactions are negligible.

- It has been found that interactions exist between NO reduction and o-DCB oxidation reactions over MnO_x-CeO_2, by comparing independent and simultaneous reaction. The presence of NO is detrimental for o-DCB oxidation, due to their competitive adsorption in Brønsted sites. However, NH_3 affects in a positive way the oxidation activity, increasing the conversion and reducing drastically the formation of byproducts. This may be attributed to the change in the acidity of the catalyst caused by NH_3 promoting MVK reaction pathways. The competence between o-DCB and NO for the same acid sites is highlighted with the decreased NO conversion in the presence of o-DCB.

- Regarding reaction mechanisms, it was concluded that o-DCB oxidation may follow two mechanisms: standard MVK mechanism and an additional mechanism consisting of a simple dechlorination reaction. On the other hand, NO reduction very likely follows preferentially ER mechanism at low temperatures, and with increasing temperature LH mechanism gains importance. It is proposed that the non-selective SCR reaction follows LH mechanism.

The present research work allowed a thorough study of the dDiNOx process over MnO_x-CeO_2, but due to experimental limitations, the proposed hypotheses still need to be proved. So, the following possible future work is proposed.

- Complete description of the kinetic behavior of the dDiNOx process over the alternative MnO_x-CeO_2 catalyst and proposal of a mechanistic equation. For this purpose, the concentrations of all compounds at the inlet and outlet of the catalytic reactor should be known.

- Analysis of the synthesis routes of MnO_x-CeO_2 catalyst in order to achieve the mixed oxide structure and determine the variables that affect in this regard. A catalyst with principally mixed oxide structure should be tested in the dDiNOx process, since it would be expected to reduce the temperature of o-DCB oxidation. In fact, new catalysts have been prepared by TQSA group changing co-precipitation method variables and using totally different synthesis routes such as redox precipitation with success. Preliminary results suggest that the aging time is a key variable for the formation of the mixed oxide structure.

- Study of the deactivation process of MnO_x-CeO_2 in order to confirm if chlorine poisoning is its source. Once the origin has been determined, promoters may be added to the catalyst to improve its behavior and avoid deactivation.

6 NOMENCLATURE

c_A	Reactant concentration, ppm
c_{A0}	Initial reactant concentration, ppm
d_p	Catalyst particle diameter, mm
K	Form factor of crystals
Q	Volumetric flow rate, L_N min^{-1}
W	Catalyst mass, g
x_A	Reactant conversion, %

6.1 GREEK LETTERS AND SYMBOLS

β	Corrected Full Width at Half Maximum, m
θ	X ray incidence angle, rad
λ	X ray wavelength, m
τ	Crystallyte size, m

6.2 ACHRONYMS AND ABBREVIATIONS

BET	Brunauer-Emmett-Teller
BJH	Brunauer-Joyner-Halenda
CEM	Controlled Evaporator-Mixer
CLD	Chemiluminiscence Detector
dDiNO_X	Technology for the simultaneous abatement of PCDD/Fs and NO_X
ER	Eley-Rideal
GHSV	Gas Hourly Space Velocity
IARC	International Agency for Research on Cancer
ICP-AES	Inductively Coupled Plasma Atomic Emission Spectroscopy
LH	Langmuir-Hinshelwood
MKV	Mars-Van Krevelen
MSD	Mass Selective Detector
MSW	Municipal Solid Waste
MWI	Municipal Waste Incineration
NDIR	Non Dispersive Infrared Detector

NO_x	Nitrogen oxides
o-DCB	1,2-dichlorobenzene
PCDD/Fs	Polichlorinated dibenzodioxins and dibenzofurans
TCD	Thermal Conductivity Detector
TEQ	Toxic Equivalency
TPD	Temperature Programmed Desorption
TPR	Temperature Programed Reduction
TQSA	*Tecnologías Químicas para la Sostenibilidad Ambiental*, Chemical Technologies for Environmental Sustainability
VOC	Volatile Organic Compounds
XRD	X-ray diffraction

7 REFERENCES

Albonetti, S., Blasioli, S., Bonelli, R., Mengou, J.E., Scirè, S., Trifirò, F., 2008. The role of acidity in the decomposition of 1,2-dichlorobenzene over TiO_2-based V_2O_5/WO_3 catalysts. Applied Catalysis A: General. 341, 18-25.

Bertinchamps, F., Attianese, A., Mestdagh, M.M., Gaigneaux, E.M., 2006. Catalysts for chlorinated VOCs abatement: Multiple effects of water on the activity of VO*x* based catalysts for the combustion of chlorobenzene. Catalysis Today. 112, 165-168.

Bertinchamps, F., Treinen, M., Blangenois, N., Mariage, E., Gaigneaux, E.M., 2005. Possitive effect of NO_X on the performances of VO_X/TiO_2-based catalysts in the total oxidation abatement of chlorobenzene. Journal of Catalysis. 230, 493-498.

Boningari, T., Koirala, R., Smirniotis, P.G., 2013. Low-temperature catalytic reduction of NO by NH_3 over vanadia-based nanoparticles prepared by flame-assisted spray pyrolysis: Influence of various supports. Applied Catalysis B: Environmental. 140-141, 289-298.

Brandenberger, S., Kröcher, O., Tissler, A., Althoff, R., 2008. The state of the art in selective catalytic reduction of NOx by ammonia using metal-exchanged zeolite catalysts. Catalysis Reviews. 50, 492-531.

Brunner, Calvin R., 1994. Hazardous waste incineration, 2nd ed. McGraw-Hill, New York.

Busca, G., Lietti, L., Ramis, G., Berti, F., 1998. Chemical and mechanistic aspects of the selective catalytic reduction of NOx by ammonia over oxide catalysts: A review. Applied Catalysis B: Environmental. 18, 1-36.

Centi, G., Cavani, F., Trifirò, F., 2001. Selective oxidation by heterogeneous catalysis, Kluwer Academic ed. 1, New York.

Chen, L., Si, Z., Wu, X., Weng, D., Wu, Z., 2015. Effect of water vapor on NH3–NO/NO2SCR performance of fresh and aged MnO*x*–NbO*x*–CeO2 catalysts. Journal of Environmental Sciences. 31, 240-247.

Cui, M., Li, Y., Wang, X., Wang, J., Shen, M., 2013. Effect of preparation method on MnOx-CeO2 catalysts for NO oxidation. Journal of Rare Earths. 31, 572-576.

Dai, Q., Bai, S., Wang, X., Lu, G., 2013. Catalytic combustion of chlorobenzene over ru-doped ceria catalysts: Mechanism study. Applied Catalysis B: Environmental. 129, 580-588.

Dai, Y., Wang, X., Dai, Q., Li, D., 2012. Effect of ce and la on the structure and activity of MnOx catalyst in catalytic combustion of chlorobenzene. Applied Catalysis B: Environmental. 111–112, 141-149.

Debecker, D.P., Bertinchamps, F., Blangenois, N., Eloy, P., Gaigneaux, E.M., 2007. On the impact of the choice of model VOC in the evaluation of V-based catalysts for the total oxidation of dioxins: Furan vs. chlorobenzene. Applied Catalysis B: Environmental. 74, 223-232.

Directive 2000/76/EC of the european parliament and of the council of 4th december 2000 on the incineration of waste, 2000.

Dvořák, R., Chlápek, P., Jecha, D., Puchýř, R., Stehlík, P., 2010. New approach to common removal of dioxins and NOx as a contribution to environmental protection. Journal of Cleaner Production. 18, 881-888.

Eigenmann, F., Maciejewski, M., Baiker, A., 2006. Selective reduction of NO by NH_3 over manganese–cerium mixed oxides: Relation between adsorption, redox and catalytic behavior. Applied Catalysis B: Environmental. 62, 311-318.

Finocchio, E., Busca, G., Notaro, M., 2006. A review of catalytic processes for the desctruction of PCDD and PCDF from waste gases. Applied Catalysis B: Environmental. 62, 12-20.

Forzatti, P., Nova, I., Enrico, T., Kustov, A., Thøgersen, J.R., 2012. Effect of operating variables on the enhanced SCR reaction over a commercial V_2O_5-WO_3/TiO_2 catalyst for stationary applications. Catalysis Today. 184, 153-159.

Gallastegi-Villa, M., 2016. $VO_x/WO_x/TiO_2$ and alternative catalysts for the simultaneous abatement of NO_x and PCDD/fs from MSW treatment plants. Ph.D. Dissertation. UPV/EHU, Leioa.

Gallezot, Pierre, 1984. X-ray techniques in catalysis, catalysis, science and technology, 1st ed. Springer-Verlag, Berlin.

Giakoumelou, I., Fountzoula, C., Kordulis, C., Boghosian, S., 2006. Molecular structure and catalytic activity of V_2O_5/TiO_2 catalysts for the SCR of NO by NH_3: In situ raman spectra in the presence of O_2, NH_3, NO, H_2, H_2O, and SO_2. Journal of Catalysis. 239, 1-12.

Goemans, M., Clarysse, P., Joannès, J., De Clercq, P., Lenaerts, S., Matthys, K., et al., 2003. Catalytic NO_X reduction with simultaneous dioxin and furan oxidation. Chemosphere. 50, 489-497.

He, C., Yu, Y., Shi, J., Shen, Q., Chen, J., Liu, H., 2015. Mesostructured cu-mn-ce-O composites with homogeneous bulk composition for chlorobenzene removal: Catalytic performance and microactivation course. Materials Chemistry and Physics. 157, 87-100.

Hetrick, C.E., Patcas, F., Amiridis, M.D., 2011. Effect of water on the oxidation of dichlorobenzene over V2O5/TiO2 catalysts. Applied Catalysis B: Environmental. 101, 622-628.

Hou, Y., Cai, G., Huang, Z., Guo, S., 2014. Effect of HCl on V2O5/AC catalyst for NO reduction by NH3 at low temperatures. Chemical Engineering Journal. 247, 59-65.

Huang, Z., Zhu, Z., Liu, Z., 2002. Combined effect of H_2O and SO_2 on V_2O_5/AC catalysts for NO reduction with ammonia at lower temperatures. Applied Catalysis B: Environmental. 39, 361-368.

International Agency for Research on Cancer, 2017. Agents classified by the IARC monographs. Available from http://monographs.iarc.fr/ENG/Classification/ (access: 26/06/2017).

Jampaiah, D., Tur, K.M., Venkataswamy, P., Ippolito, S.J., Sabri, Y.M., Tardio, J.,Suresh K., et al., 2015. Catalytic oxidation and adsorption of elemental mercury over nanostructured CeO2–MnO*x* catalyst. RSC Advances. 5, 30331-30341.

Jones, J., Ross, J.R.H., 1997. The development of supported vanadia catalysts for the combined catalytic removal of the oxides of nitrogen and of chlorinated hydrocarbons from flue gases. Catalysis Today. 35, 97-105.

Kang, M., Park, E.D., Kim, J.M., Yie, J.E., 2007. Manganese oxide catalysts for NOx reduction with NH3 at low temperatures. Applied Catalysis A: General. 327, 261-269.

Kapteijn, F., Singoredjo, L., Andreini, A., 1994. Activity and selectivity of pure manganese oxides in the selective catalytic reduction of nitric oxide with ammonia. Applied Catalysis B: Environmental. 3, 173-189.

Khodakov, A., Olthof, B., Bell, A.T., Iglesia, E., 1999. Structure and catalytic properties of supported vanadium oxides: Support effects on oxidative dehydrogenation reactions. Journal of Catalysis. 181, 205-216.

Kondratenko, E.V., Ovsitser, O., Radnik, J., Schneider, M., Kraehnert, R., Dingerdissen, U., 2007. Influence of reaction conditions on catalyst composition and selective/non-selective reaction pathways of the ODP reaction over V_2O_3, VO_2 and V_2O_5 with O_2 and N_2O. Applied Catalysis A: General. 319, 98-110.

Ley 22/2011, de 28 de julio, de residuos y suelos contaminados, Jefatura del Estado, 2011.

Li, J., Chen, J., Ke, R., Luo, C., Hao, J., 2007. Effects of precursors on the surface Mn species and the activities for NO reduction over MnO*x*/TiO2 catalysts. Catalysis Communications. 8, 1896-1900.

Lietti, L., Nova, I., Forzatti, P., 2000. Selective catalytic reduction (SCR) of NO by NH3 over TiO2-supported V2O5–WO3 and V2O5–MoO3 catalysts. Topics in Catalysis. 11, 111-122.

Liu, C., Shi, J., Gao, C., Niu, C., 2016. Manganese oxide-based catalysts for low-temperature selective catalytic reduction of NOx with NH3: A review. Applied Catalysis A: General. 522, 54-69.

Liu, H., Kong, S., Liu, Y., Zeng, H., 2012. Pollution control technologies of dioxins in municipal solid waste incinerator. Procedia Environmental Sciences. 16, 661-668.

Liu, Z., Yi, Y., Zhang, S., Zhu, T., Zhu, J., Wang, J., 2013. Selective catalytic reduction of NO_x with NH_3 over Mn-Ce mixed oxide catalyst at low temperatures. Catalysis Today. 216, 76-81.

Ma, X., Feng, X., He, X., Guo, H., Lü, L., 2011. Preparation, characterization and catalytic behavior of hierarchically porous CuO/α-Fe2O3/SiO2 composite material for CO and *o*-DCB oxidation. Journal of Natural Gas Chemistry. 20, 618-622.

Machida, M., Uto, M., Kurogi, D., Kijima, T., 2000. MnOx-CeO2 binary oxides for catalytic NOx sorption at low temperatures. Sorptive removal of NOx. Chemistry of Materials. 12, 3158-3164.

Marbán, G., Valdés-Solís, T., Fuertes, A.B., 2004. Mechanism of low-temperature selective catalytic reduction of NO with NH3 over carbon-supported Mn3O4: Role of surface NH3 species: SCR mechanism. Journal of Catalysis. 226, 138-155.

McKay, G., 2002. Dioxin characterisation, formation and minimisation during municipal solid waste (MSW) incineration: Review. Chemical Engineering Journal. 86, 343-368.

Nova, I., Lietti, L., Tronconi, E., Forzatti, P., 2000. Dynamics of SCR reaction over a TiO_2-supported vanadia–tungsta commercial catalyst. Catalysis Today. 60, 73-82.

Picasso, G., Cruz, R., Kou, M.R.S., 2015. Preparation by co-precipitation of Ce–Mn based catalysts for combustion of n-hexane. Materials Research Bulletin. 70, 621-632.

Qi, F., Xiong, S., Liao, Y., Dang, H., Yang, S., 2015. A novel dual layer SCR catalyst with a broad temperature window for the control of NO*x* emission from diesel bus. Catalysis Communications. 65, 108-112.

Qi, G., Yang, R.T., 2003. Performance and kinetics study for low-temperature SCR of NO with NH3 over MnOx–CeO2 catalyst. Journal of Catalysis. 217, 434-441.

Qi, G., Yang, R.T., Chang, R., 2004. MnO_x-CeO_2 mixed oxides prepared by co-precipitation for selective catalytic reduction of NO with NH_3 at low temperatures. Applied Catalysis B: Environmental. 51, 93-106.

Reimann, D.O., 2013. CEWEP energy report III: Status 2007-2010. Confederation of European Waste-to-Energy Plants.

Saleh, F.S., Rahman, M.M., 2009. Oxidative destruction of *o*-DCB on supported manganese oxide catalyst. Journal of Hazardous Materials. 162, 1574-1577.

Sing, K.S.W., Everett, D.H., Haul, R.A.W., Moscou, L., Pierotti, R.A., Rouquérol, J., et al., 1985. Reporting physisorption data for gas/solid systems with special reference to the determination of surface area and porosity. Pure and Applied Chemistry. 57, 603-619.

Sun, P., Wang, W., Dai, X., Weng, X., Wu, Z., 2016. Mechanism study on catalytic oxidation of chlorobenzene over MnxCe1-xO2/H-ZSM5 catalysts under dry and humid conditions. Applied Catalysis B: Environmental. 198, 389-397.

Tang, X., Hao, J., Xu, W., Li, J., 2007. Low temperature selective catalytic reduction of NO_x with NH_3over amorphous MnO_x catalysts prepared by three methods. Catalysis Communications. 8, 329-334.

Tang, X., Li, J., Sun, L., Hao, J., 2010. Origination of N_2O from NO reduction by NH_3 over β-$MnO_2$and α-mn_2O_3. Applied Catalysis B: Environmental. 99, 156-162.

Tang, X., Li, Y., Huang, X., Xu, Y., Zhu, H., Wang, J., et al., 2006. MnOx–CeO2 mixed oxide catalysts for complete oxidation of formaldehyde: Effect of preparation method and calcination temperature. Applied Catalysis B: Environmental. 62, 265-273.

Topsoe, N.Y., Topsoe, H., Dumesic, J.A., 1995. Vanadia/titania catalysts for selective catalytic reduction (SCR) of nitric-oxide by ammonia: I. combined temperature-programmed *in-situ* FTIR and on-line mass-spectroscopy studies. Journal of Catalysis. 151, 226-240.

Wachs, I.E., 2011. The generality of surface vanadium oxide phases in mixed oxide catalysts. Applied Catalysis A: General. 391, 36-42.

Wachs, I.E., 1990. Molecular structures of surface vanadium oxide species on titania supports. Journal of Catalysis. 124, 570-573.

Wachs, I.E., Chen, Y., Jehng, J., Briand, L.E., Tanaka, T., 2003. Molecular structure and reactivity of the group V metal oxides. Catalysis Today. 78, 13-24.

Wachs, I.E., Deo, G., Weckhuysen, B.M., Andreini, A., Vuurman, M.A., Boer, M.D., et al., 1996. Selective catalytic reduction of NO with NH_3 over supported vanadia catalysts. Journal of Catalysis. 161, 211-221.

Wang, J., Wang, X., Liu, X., Zeng, J., Guo, Y., Zhu, T., 2015. Kinetics and mechanism study on catalytic oxidation of chlorobenzene over V_2O_5/TiO_2 catalysts. Journal of Molecular Catalysis A: Chemical. 402, 1-9.

Wang, X., Kang, Q., Li, D., 2008. Low-temperature catalytic combustion of chlorobenzene over MnOx–CeO2 mixed oxide catalysts. Catalysis Communications. 9, 2158-2162.

Waste-to-Energy Research and Technology Council, 2017. Current state of waste management in Germany. Available from http://www.wtert.eu/default.asp?Menue=14&ShowDok=30 (access: 26-06-2017).

Wei, Y., Sun, Y., Su, W., Liu, J., 2015. MnO2 doped CeO2 with tailored 3-D channels exhibits excellent performance for NH3-SCR of NO. RSC Advances. 5, 26231-26235.

Wielgosiński, G., Grochowalski, A., Machej, T., Pajak, T., Cwiakalski, W., 2007. Catalytic destruction of 1,2-dichlorobenzene on V_2O_5-WO_3/al_2O_3-TiO_2 catalyst. Chemosphere. 67, 150-154.

Wu, Z., Jiang, B., Liu, Y., Wang, H., Jin, R., 2007a. DRIFT study of manganese/titania-based catalysts for low-temperature selective catalytic reduction of NO with NH3. Environmental Science Technology. 41, 5812-5817.

Wu, Z., Jiang, B., Liu, Y., Zhao, W., Guan, B., 2007b. Experimental study on a low-temperature SCR catalyst based on MnOx/TiO2 prepared by sol–gel method. Journal of Hazardous Materials. 145, 488-494.

Wu, Z., Jin, R., Liu, Y., Wang, H., 2008. Ceria modified MnO_x/TiO_2 as a superior catalyst for NO reduction with NH_3 at low-temperature. Catalysis Communications. 9, 2217-2220.

Xu, L., Li, X., Crocker, M., Zhang, Z., Zhu, A., Shi, C., 2013. A study of the mechanism of low-temperature SCR of NO with NH3 on MnOx/CeO2. Journal of Molecular Catalysis A: Chemical. 378, 82-90.

Xue, W., Jian, W., Tingyu, Z., 2013. Coupled control of chlorobenzene and NO over V_2O_5/TiO_2 catalyst in NH_3-SCR reaction. Advanced Materials Research. 8, 83-86.

Yao, X., Ma, K., Zou, W., He, S., An, J., Yang, F., et al., 2017. Influence of preparation methods on the physicochemical properties and catalytic performance of MnOx-CeO2 catalysts for NH3-SCR at low temperature. Chinese Journal of Catalysis. 38, 146-159.

Zhan, W., Zhang, X., Guo, Y., Wang, L., Guo, Y., Lu, G., 2014. Synthesis of mesoporous CeO2-MnOx binary oxides and their catalytic performances for CO oxidation. Journal of Rare Earths. 32, 146-152.